Journal of Geodynamics 74 (2014) 32–55

Contents lists available at ScienceDirect

Journal of Geodynamics

journal homepage: http://www.elsevier.com/locate/jog

Late Cenozoic faulting in SW Bulgaria: Fault geometry, kinematics and driving stress regimes. Implications for late orogenic processes in the Hellenic hinterland

Markos D. Tranos[a,*], Olivier Lacombe[b,c]

[a] Department of Geology, Aristotle University of Thessaloniki, 54124 Thessaloniki, Greece
[b] UPMC Univ Paris 06, UMR 7193, ISTEP, F-75005 Paris, France
[c] CNRS, UMR 7193, ISTEP, F-75005 Paris, France

ARTICLE INFO

Article history:
Received 19 August 2013
Received in revised form
18 November 2013
Accepted 9 December 2013
Available online 16 December 2013

Keywords:
Transpression
Collision
Late orogenic faulting
Lateral extrusion
Extension
Neotectonics
Strouma River

ABSTRACT

We investigate the geometry and kinematics of the faults exposed in basement rocks along the Strouma River in SW Bulgaria as well as the sequence of faulting events in order to place constraints on the Cenozoic kinematic evolution of this structurally complex domain. In order to decipher the successive stress fields that prevailed during the tectonic history, we additionally carried out an analysis of mesoscale striated faults in terms of paleostress with a novel approach. This approach is based on the P–T axes distribution of the fault-slip data, and separates the fault-slip data into different groups which are characterized by kinematic compatibility, i.e., their P and T axes have similar orientations. From these fault groups, stress tensors are resolved and in case these stress tensors define similar stress regimes (i.e., the orientations of the stress axes and the stress shape ratios are similar) then the fault groups are further unified. The merged fault groups after being filled out with those fault-slip data that have not been incorporated into the above described grouping, but which present similar geometric and kinematic features are used for defining the final stress regimes. In addition, the sequence of faulting events was constrained by available tectonostratigraphic data.

Five faulting events named D1, D2, D3, D4 and D5 are distinguished since the Late Oligocene. D1 is a pure compression stress regime with σ_1 stress axis trending NNE-SSW that mainly activated the WNW-ESE to ENE-WSW faults as reverse to oblique reverse and the NNW-SSE striking as right-lateral oblique contractional faults during the Latest Oligocene-Earliest Miocene. D2 is a strike-slip – transpression stress regime with σ_1 stress axis trending NNE-SSW that mainly activated the NNW-SSE to N-S striking as right-lateral strike-slip faults and the ENE-WSW striking faults as left-lateral strike-slip ones during the Early-Middle Miocene. D3 extensional event is associated with a NW-SE to WNW-ESE extension causing the activation of mainly low-angle normal faults of NE-SW strike and NNE-SSW to NNW-SSE striking high-angle normal faults. D4 is an extensional event dated from Late Miocene to Late Pliocene. It activated NNW-SSE to NW-SE faults as normal faults and E-W to WNW-ESE faults as right-lateral oblique extensional faults. The latest D5 event is an N-S extensional stress regime that dominates the wider area of SW Bulgaria in Quaternary times. It mainly activated faults that generally strike E-W (ENE-WSW and WNW-ESE) normal faults, along which fault-bounded basins developed. The D1 and D2 events are interpreted as two progressive stages of transpressional tectonics related to the late stages of collision between Apulia and Eurasia plates. These processes gave rise to the lateral extrusion of the Rhodope and Balkan regions toward the SE along the Strouma Lineament. The D3 event is attributed to the latest stage of this collision, and represents the relaxation of the overthickened crust along the direction of the lateral extrusion. The D4 and D5 events are interpreted as post-orogenic extensional events related to the retreat of the Hellenic subduction zone since the Late Miocene and to the widespread back-arc Aegean extension still prevailing today.

1. Introduction

In the past two decades, geological processes related to late-collisional deformation that control the final configuration and shape of orogens have been an attractive research subject through which a better understanding of the (late) evolution of the orogens

* Corresponding author. Tel.: +30 2310998830; fax: +30 2310998482.
E-mail addresses: tranos@geo.auth.gr, tranosgeo@gmail.com (M. D. Tranos).

0264-3707/$ – see front matter © 2013 Elsevier Ltd. All rights reserved.
http://dx.doi.org/10.1016/j.jog.2013.12.001

was achieved. An area of special interest is the Aegean domain where late-and post-orogenic processes within the Hellenic orogen gave rise to the well-known Cyclades metamorphic core complexes (Jolivet and Brun, 2010; Jolivet et al., 2010; and reference therein).

Several issues, however, such as the type and modes of activation of fault structures formed during the late- and post-collisional stages, the lasting periods of the different faulting events as well as their driving stresses still remain under debate. In the hinterland part of the orogen, these issues are much more difficult to decipher because the post-orogenic processes have significantly obliterated the fault structures that were active during the late collisional stage. The question is especially striking in those parts of orogens that were shortened between two divergent mountain belts and/or where the plate boundary includes both advancing and retreating parts through time.

An example of such complex setting is SW Bulgaria that underwent shortening between the SW-verging Dinarides-Hellenides and the NNE to N-verging Balkanides (Fig. 1a). Since both of these mountain belts are characterized by a complex deformation history, the late orogenic evolution of SW Bulgaria, which is mostly related to faulting deformation during the Late Cenozoic, is also complex (Fig. 1b). According to Zagorchev (1992), the late Cenozoic faulting deformation of SW Bulgaria involves multiple activations of many differently oriented faults that were active in different geological times and thus corresponds to different faulting events.

In general, the studies conducted in neighboring areas, such as West and South Bulgaria, Central and Eastern Macedonia, Eastern Thrace and SW Black Sea propose different deformational models to account for the faulting processes that took place since the end of nappe stacking. More precisely, they suggest either that (a) the extension, in general, began in the Late Miocene (Mercier et al., 1989; Zagorchev, 1992; Dinter and Royden, 1993; Tranos, 1998; Westaway, 2006) following a transpressional stress regime (Tranos, 2004; Tranos et al., 2008 for SW Bulgaria; Tranos, 1998, 2011; Tranos et al., 1999 for Central and Eastern Macedonia; Koukouvelas and Doutsos, 1990 for Thrace; Görür and Okay, 1996 for Eastern Thrace; Doglioni et al., 1996; Sinclair et al., 1997 for eastern Balkans) or that (b) since the Eocene-early Oligocene the extension, reflecting orogen collapse after collisional stacking, has been continuing up to the present (Bonev et al., 1995; Kilias and Mountrakis, 1998; Kilias et al., 1999; Kounov et al., 2004; Brun and Sokoutis, 2007). The idea of a continuity of the extension since the Eocene, however, is not shared by Georgiev et al. (2010) who separate the Eocene-Oligocene extension from the Miocene extension. It is worth mentioning that in this paper the term transpression is used as a stress term (i.e., as initially defined by Harland, 1971 and adapted by Marrett and Peacock, 1999). As a result, when deformation is described in terms of strain the term oblique contraction as suggested by Marrett and Peacock (1999) is used instead of transpression.

In addition, other studies made in West and South Bulgaria indicated that parts of the Rhodope massif and Serbo-Macedonian massif have already been exhumed by a syn-orogenic extension that took place after the pre-Late Cretaceous nappe stacking and before the Early Oligocene magmatism (Graf, 2001; Kounov et al., 2004; Bonev et al., 2006; Burg, 2012).

Although the current state of stress and extensional fault kinematics as shown in Fig. 2 is rather well known (Tranos et al., 2006; Meyer et al., 2002, 2007), the general geometry and kinematics of the differently oriented faults in the basement rocks of SW Bulgaria (Fig. 1b) remain to be properly characterized and constrained in order to define the multiple activations of the faults. The twofold aim of this paper is (1) to define the geometry and kinematics of the differently oriented faults exposed in the basement rocks in the region of SW Bulgaria and mainly along the Struma Lineament (i.e., a more than 800-km-long tectonic feature that trending NNW-SSE controls the course of Struma River), and (2) to establish the sequence of the successive fault movements, as well as the different stress regimes that drove faulting deformation though time. To this latter aim, our results will be combined with tectonostratigraphic data available from literature in order to gain better time constraints on the faulting evolution of SW Bulgaria since the Oligocene, within the Neogene tectonic framework of the Eastern Mediterranean and Aegean Sea.

2. Geological setting

At the regional scale, the orogenic fabric of central Balkan Peninsula is dominated by the NW-SE trending alpine Dinaro-Hellenic mountain belt and the E-W trending Balkan mountain belt; the latter consists in the southern part of the S-shaped Romanian Carpathian-Balkan belt around the Moesian platform (Fig. 1a). In addition, the orogenic fabrics of these two mountain belts form a V-shape with apex in the western edge of the Moesian platform and opening toward the SE, i.e., the North Aegean Sea.

The study area in SW Bulgaria forms the exposed hinterland of these mountain belts. It is dominated by a more than 800-km-long inherited tectonic feature known as the Strouma Lineament (Bonchev, 1958; Zagorchev, 1992; Tranos et al., 2008; Tranos, 2011) that controls a large portion of the course of the Strouma (Strymon) River. This structure strikes NNW-SSE and cuts through several Alpine tectonic zones in former Yugoslavia, Bulgaria, and Greece (Fig. 1a). In SW Bulgaria, several narrow depocentres (i.e. the Dzherman, Blagoevgrad, Simitli, and Sandanski) have developed (Zagorchev, 1992) along this lineament during the Neogene forming the northern part of the Strouma/Strymon graben system, herein referred to as the Blagoevgrad–Sandanski graben system. Further to the south, in Greece, the Strumon Lineament has been firstly reported as “Die Strumonlinie” from Kockel and Walther (1965) to separate the Serbo-Macedonian massif from the Rhodope massif along which the Strymon basin, filled with Neogene and Quaternary terrestrial sediments and terminated in the North Aegean Sea, forms the southern part of the Strouma/Strymon graben system (Tranos, 2011).

More precisely, the study area is located along the Strouma River from the Kyustendil region in the north to the Kresna region in the south. It consists of a high grade metamorphic domain (Fig. 1). It is also the region where the NNW-SSE trending Vardar-Axios, Circum Rhodope Belt Thrust System (CRBTS) and the Serbo-Macedonian massif (related to SW-verging alpine Dinaric-Helenic mountain belt) come into contact with the Rhodope massif and the N-verging Balkan mountain belt (Fig. 1a).

The geology of SW Bulgaria has been thoroughly described by Zagorchev (2001). According to this author the study area includes Pre-Paleozoic and Paleozoic high grade (amphibolitic facies) metamorphic rocks that form: (a) the mountainous domain E and SE of Strouma River which belongs to the Rhodopian Supergroup and the Ograzhdenian (Pre-Rhodopian) Supergroup, and (b) the mountainous domain SW of the town of Kyustendil (i.e., Mt Osogovo), which belongs to the Osogovo Formation. These rocks were intruded by several large granitoid bodies and were unconformably overlain by the Lower Paleozoic greenschist-facies diabase and phyllitoid complex (mainly the Frolosh Formation). In turn, these were intruded by the Paleozoic Strouma diorite. However, this geology has been significantly revised by the recent works of Bonev et al. (1995), Kounov et al. (2004, 2010, 2011) and Burg (2012): among recent intepretations are that the crystalline rocks are not Pre-Paleozoic but younger than Paleozoic, that the Osogovo Formation has been metamorphosed during the Cretaceous, that the Frolosh Formation consists of ophiolitic materials, that the Struma Diorites represent a magmatic arc complex of Ediacaran-Early Cambrian age, and that

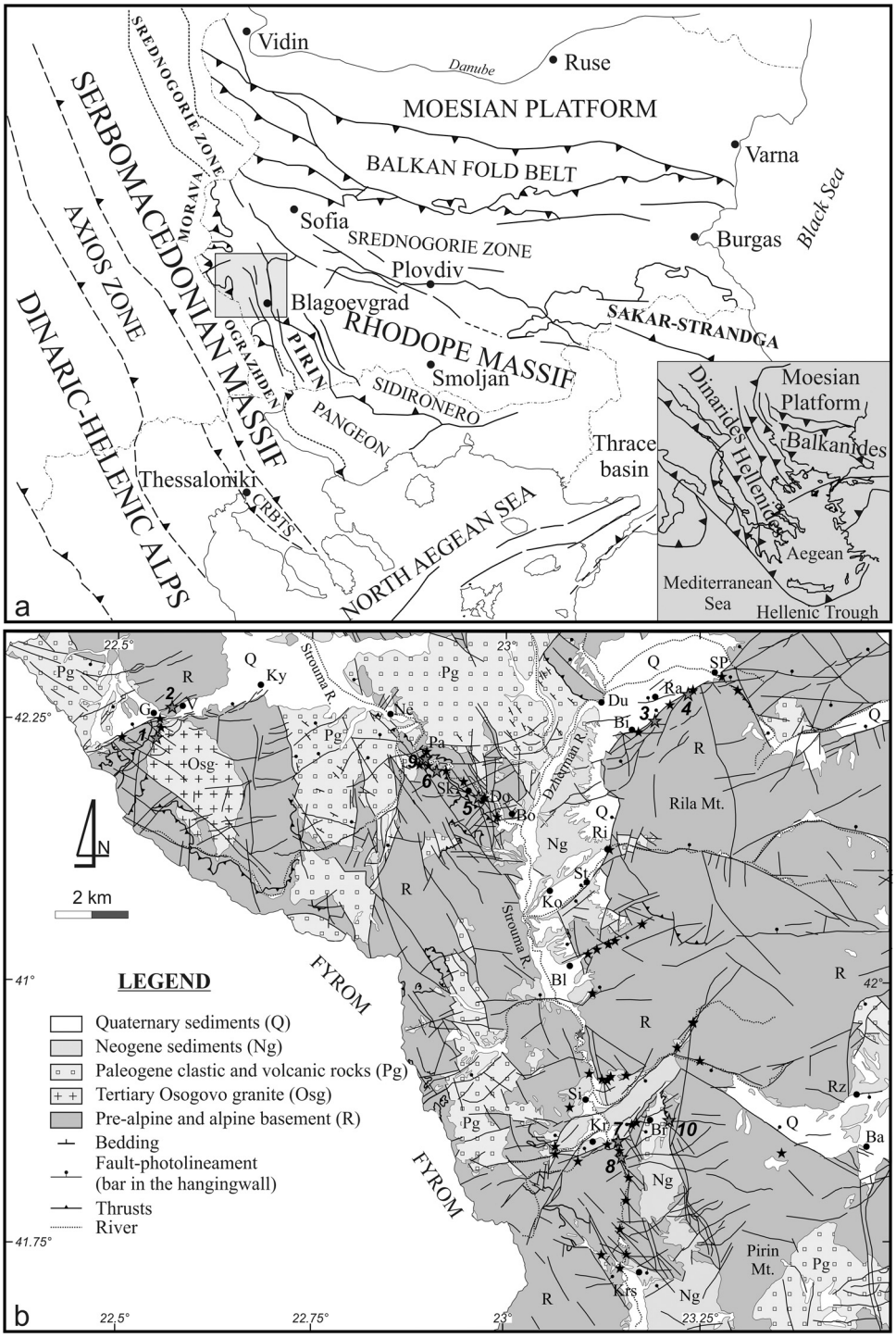

Fig. 1. (a) Map indicates the study area, its position in relation to the main Alpine orogenic elements of the wider area and the general geotectonic framework of the eastern Mediterranean region, (b) geological and structural map of SW Bulgaria (compiled from satellite imagery analysis, field mapping, and published geological maps 1:100.000 (Zagorchev, 1989, 1991; Marinova and Zagorchev, 1990a,b). Black stars indicate locations of sites of measurements; gray stars with numbers indicate sites where photographs shown in Fig. 4 have been taken; Ba: Bansko, Bi: Bistritsa, Bl: Blagoevgrad, Bo: Bobochevo, Do: Dobrovo, G: Garliano, D: Doupnitsa, Ko: Kocerinovo, Kr: Kroupnik, Krs: Kresna, Ky: Kyustendil, Pa: Pastouch, Ri: Rila, Ra: Racilevo, Ne: Nevestino, Rz: Razlog, Si: Simitli, S: Stob, Sk: Skrinio, SP: Saparevo, V: Vrattsa, FYROM: Former Yugoslavian Republic of Macedonia.

the Ograzden rocks have been metamorphosed during the Variscan time. The details of the complex geology of the region are however far beyond the scope of the present paper and because of this any further attempt to approach in more detail the pre-Cenozoic geology is not further considered. Even more, the Mesozoic rocks are exposed in limited outcrops west of Strouma River, whereas the Paleogene sediments outlasting the Late Oligocene crop out extensively along the Strouma River, i.e., in the section between Doupnitsa and Kyustendil (Fig. 1b).

More precisely, the Paleogene sediments contain of: (a) Middle Eocene continental clastic sediments which pass upwards to Late Eocene-Lower Oligocene turbidities of deepwater environment (Moskovski and Shopov, 1965) and which were intruded by volcanic rocks in the Early Oligocene (Harkovska and Pecskay, 1997),

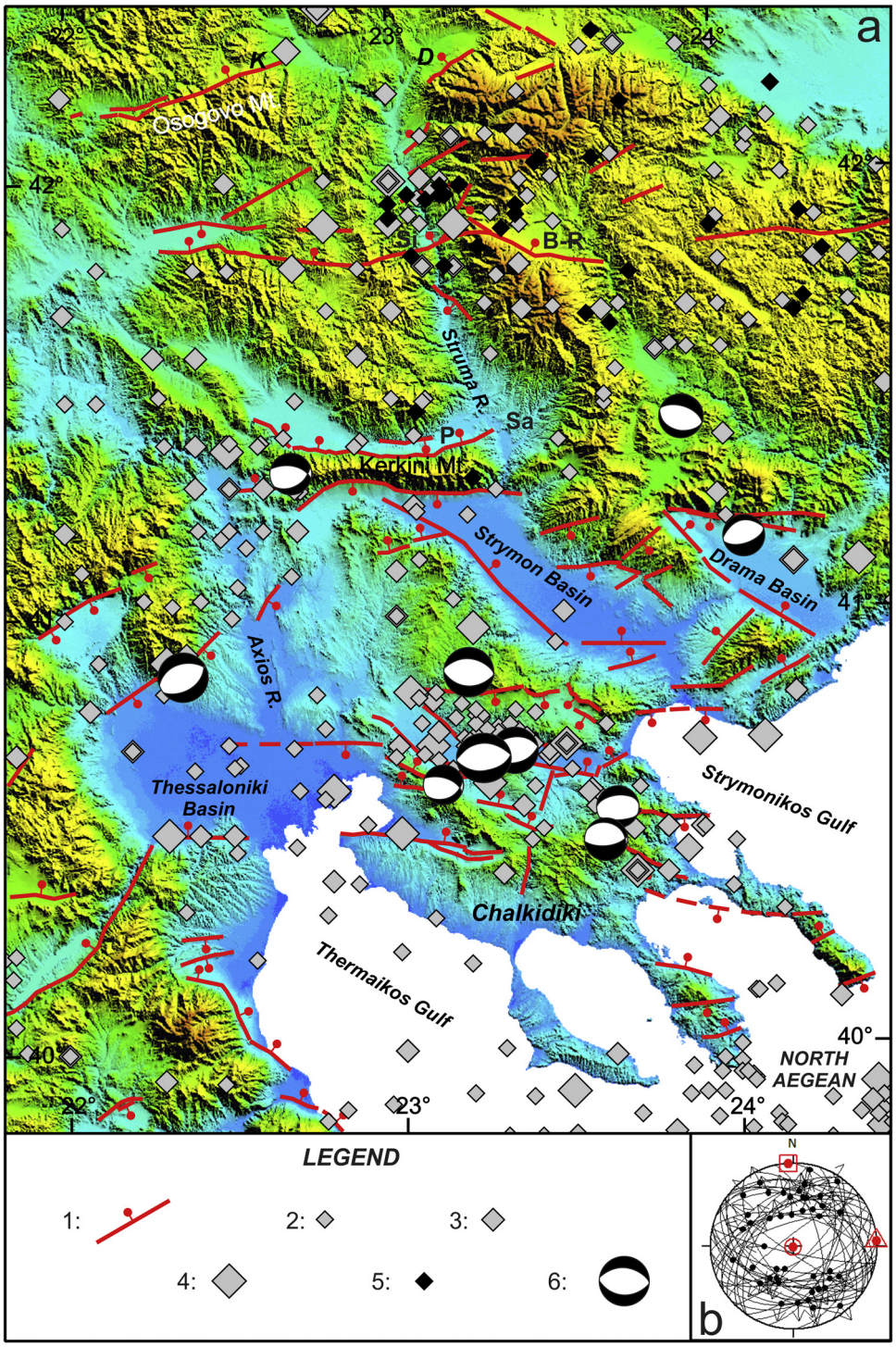

Fig. 2. (a) Seismotectonic map of SW Bulgaria, Central Macedonia (northern Greece) and FYROM. It shows the (1) main neotectonic faults, (2, 3, 4 and 5) seismicity and (6) focal mechanisms of some published earthquake events ($M \geq 5$). Explanation: 1. Neotectonic faults, 2, 3, 4. Earthquakes of period 1901–2010 (catalog of Seismological Station of Aristotle University of Thessaloniki, http://geophysics.geo.auth.gr/ss/station_index.html), 2. Epicenters of earthquakes with $4 < M \leq 5$, 3. Epicenters of earthquakes with $5 < M \leq 6$, 4. Epicenters of earthquakes with $M > 6$, 5. Epicenters of earthquakes with a range in magnitude of 3.0 to 5.7 spanning the period 1956 to 1998 (Kotzev et al., 2006), 6. Beach balls of focal mechanisms of large earthquake events ($M \geq 5$) associated with normal faults (from Kiratzi, 2010), B-R: Bansko-Razlog, D: Doupnitsa, K: Kyustendil, P: Petritsi, Sa: Sandanski, Si: Simitli, (b) the P–B–T axes as defined by the focal mechanisms of the earthquakes (5) shown in (a) with the aid of the Win-Tensor software (Delvaux, 2011). P, B and T axes are shown with circles, triangles and squares respectively.

and (b) Upper Oligocene-Early Miocene terrigenous coal-bearing sediments that unconformably overlie the former sedimentary sequence, possibly due to a NE-SW compression that gave rise to inversion of the basins associated with the end of sedimentation and to folding and faulting of the sediments with reverse and strike-slip faults (Moskovski, 1968a,b, 1969; Moskovski and Harkovska, 1973). On the basis of fission-track dating and modeling of thermal history, Graf (2001) stated that the inversion of the basins could have begun at 25 ± 5 Ma. However, Bakalov and Zelev (1996) report that the sedimentation from the Early Oligocene to Late Oligocene-Miocene was continuous and Kounov et al. (2004) attributed the basin inversion to the ongoing extension

and the exhumation of the extensional core complex; this points to a complex Tertiary regional geology that still remains a matter of debate.

During the Neogene, several narrow depocenters, (i.e., the Dzherman, Blagoevgrad, Simitli, and Sandanski) have developed in the area (Zagorchev, 1992) represented by the Strouma (or Blagoevgrad-Sandanski) graben system along the Strouma Lineament and the WNW-ESE Bansko-Razlog graben along the Predela-Bansko fault. The oldest sediments deposited in the Struma–Strimon Basin contain Middle Miocene mammal fossils (Kojumdgieva et al., 1982). In general, the Neogene sedimentation involves three sedimentary cycles (Nedjalkov et al., 1988; Zagorchev, 1992): (a) the Late Badenian-Sarmatian that consists of red polymictic conglomerates, laterally passing (?) into greenish or reddish siltstones and sandstones with clay interbeds, (b) the Meotian-earliest Pontian that produced whitish or yellowish alluvial sand and clay interbedded with pebble gravel lenses (Sandanski and Simitli Formations) and, (c) the Pontian-Pliocene that is characterized by the well sorted conglomerates and sandstones of the Barakovo Formation (Blagoevgrad graben) and Kalimantsi Formation (Simitli and Sandanski graben).

Since the Quaternary, a younger cycle of sedimentation was recognized (Vrablianski, 1974), which includes the deposition of poorly sorted proluvial deposits along mountain fronts such as in the eastern parts of Blagoevgrad graben and the NW edge of Rila Mt., as well as alluvial deposits along the Strouma River and its tributaries.

In summary, the Tertiary alpine orogenic events mainly include a Cretaceous to Paleocene nappe stacking episode followed by post-Middle Cretaceous to pre-Middle Oligocene extension (Graf, 2001; Kounov et al., 2004; Burg, 2012). This extension gave rise to a widespread tectonic denudation associated with large extensional shear zones like the "Gabrov Dol ductile normal fault" (Bonev et al., 1995) or detachments, e.g., the Ruen (Graf, 2001), Eleshnitsa, Dragovishtitsa (Graf, 2001; Kounov et al., 2004) and the Vlahina–Maleshevo Detachment Fault (Peychev et al., 2012). These detachments, however, have been inactive after the Late Eocene-Early Oligocene because they have been cut by the unmetamorphosed and generally undeformed calc-alkaline granites (Osogovo granite) and rhyolites that intruded the tectonostratigraphic column of the region in Early to Middle Oligocene times [30.6 ± 1.6 Ma (Graf, 2001); 31 ± 3 Ma and 31 ± 2 Ma (Kounov et al., 2004; 32.3–31.5 Ma (Harkovska and Pecskay, 1997)].

According to Zagorchev (1992) the late Cenozoic faulting deformation includes the following faulting events since the Oligocene: a Middle Oligocene (?) and earliest Miocene-Badenian shortening events associated with thrusting, and a Middle Oligocene-Early Miocene, Late Badenian-Meotian, Pontian-Romanian, and Pleistocene-Holocene extensional events that caused normal faulting. The most recent studies dealing with Tertiary faulting of the region are only those of Tranos et al. (2008) and Kounov et al. (2011); although these studies led to different conclusions, they both emphasize the multiple activation of the faults.

Tranos et al. (2008) studied faulting in the Simitli region (Fig. 1b) and defined: (a) a Late Oligocene-Early Miocene transpression-pure compression stress regime with NNE–SSW contraction (D_A event), (b) a strike-slip to transtension stress regime in Early-Middle Miocene (D_B event), (c) a transtension to pure extension stress regime in Middle-Late Miocene (D_1 event), (d) a NE-SW radial-pure extension in Late Miocene-Pliocene (D_2 event) and N-S extension in Quaternary (D_3 event).

On the other hand, the paleostress analysis in the Kraishte area, SW Bulgaria by Kounov et al. (2011) has led to define four regional stress tensors: Early Cretaceous N-S compression (D1), Middle Eocene-Early Oligocene ENE-WSW extension (D2), Early Oligocene NE-SW extension (D3), and Late Oligocene-Early Miocene NNW-SSE transtension (D4).

From the afore-mentioned works and their controversies it is obvious that the fault network of the region is complex, including reactivation of many faults inherited from the successive late orogenic stages (Zagorchev, 1992).

Finally, new paleomagnetic data have shown no significant post-Eocene rotation of the Moesian platform and Rhodope with respect to Eurasia, therefore confirming the stability of this region (Van Hinsbergen et al., 2008). This conclusion is also supported by the recorded structural data in SW Bulgaria (Georgiev et al., 2010). On the other hand, Dimitriadis et al. (1998) reported that Greek Rhodope (all or parts of it) may have been rotated by 13° clockwise during the Late Oligocene-Early Miocene despite the fact that these rotations have not been verified by the recorded structural data (Kolokotroni and Dixon, 1991; Dinter and Royden, 1993; Dinter, 1998). In addition, clockwise rotations after the Middle Miocene mainly refer to the Serbo-Macedonian massif of Northern Greece (Dimitriadis et al., 1998).

3. Faulting of SW Bulgaria

3.1. Fault pattern at a large scale

Bulgaria is an intracontinental region that shares similar seismotectonic characteristics with the adjacent intensely stretched Aegean domain (Tranos et al., 2006) (Fig. 2). The N-S stretching that dominates the Aegean has been demonstrated in Northern Greece (Mountrakis et al., 2006) and SW Bulgaria where it led to km-long active normal faults striking E-W on average (i.e., from WNW-ESE to WSW-ENE) (Tranos et al., 2006). These faults are distributed throughout the region, but they are few and segmented, bounding small grabens that cut across the orogenic fabric of the Dinaric-Hellenic belt as well as the Rhodope and Balkan belt (Fig. 2). Nonetheless, these grabens are a few tens of kilometers long at most, i.e., much smaller than the large fault-bounded basins of Northern and central Greece. Accordingly, the deformation rates in Northern Greece and Bulgaria are much smaller than within the Aegean and appear to decrease northward. GPS measurements indicate 2–3 mm/year of N-S extension across Bulgaria and northern Greece (McClusky et al., 2000; Kahle et al., 2000) of which at most 1 mm/year is absorbed in Bulgaria (Kotzev et al., 2006).

The fault pattern of SW Bulgaria (Fig. 1b) as identified from 1:100.000 scale geological maps (Zagorchev, 1989, 1991; Marinova and Zagorchev, 1990a,b), interpreted from Landsat satellite imagery and controlled by field observations is more complex. In particular, it is characterized by the presence of many km-long faults striking NNW-SSE to NW-SE, NE-SW to ENE-WSW and WNW-ESE. The NNW-SSE to NW-SE trending faults are mostly defined along the Strouma River and controls the outcrops of the Late Paleogene and Neogene rocks against the basement. They are the most commonly mapped faults in the afore-mentioned geological maps, but are hardly defined on the Landsat imagery. On the other hand, the NE-SW to ENE-WSW trending faults are the most common and prevalent lineaments on the Landsat imagery that bound long narrow basins filled with Neogene and Quaternary sediments such as the Kyustendil, Doupnitsa, Kroupnik and Rila-Stob basins (Tranos et al., 2006). Finally, the WNW to ESE faults are the most prevalent structures in the part east of the Strouma River where they form large rectilinear lineaments limiting narrow basins such as the Predela-Bansko basin.

3.2. Mesoscale faults

The microstructural investigation of the study area includes the analysis of slip along mesoscale faults that have been recorded in

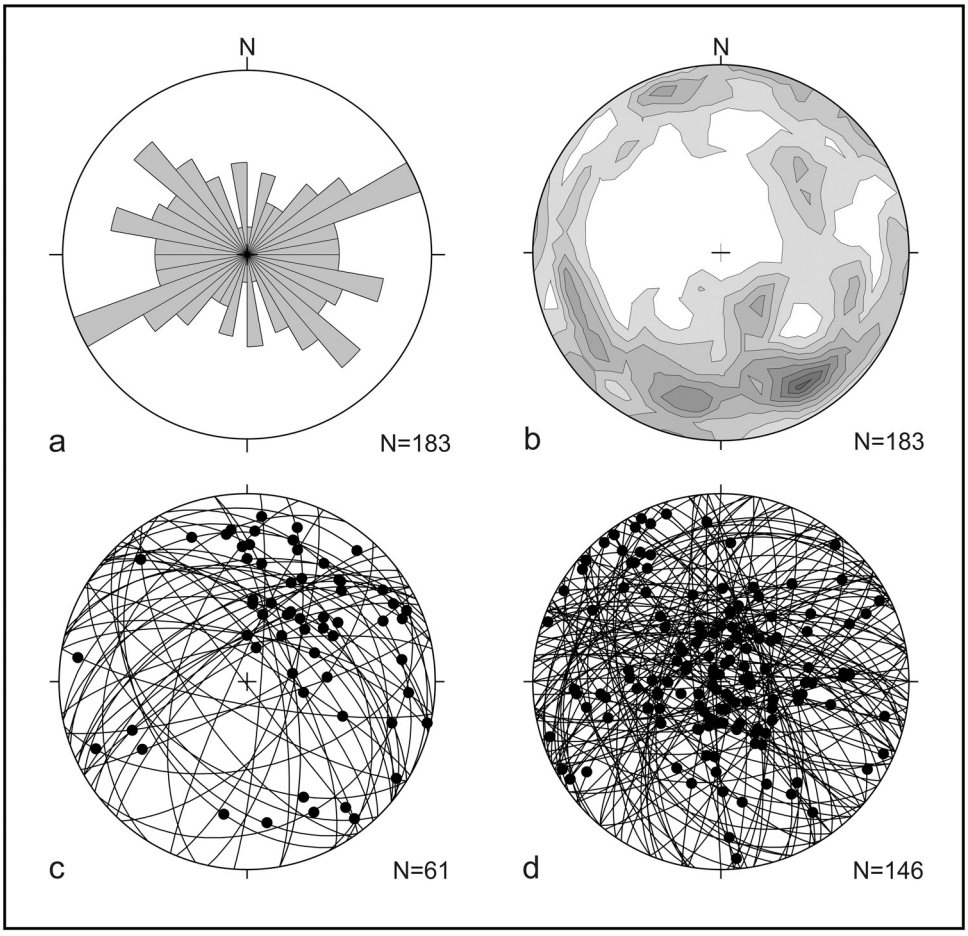

Fig. 3. (a) Strike rose-diagram and pole diagram of the recorded mesoscale faults that contain slickenlines, In (b) the density contours are at 0.5, 1, 1.5, . . ., 4 with a maximum density at 4.21. (c, d) Lower hemisphere, equal area stereographic projection of (c) the contractional fault-slip data ($N = 61$) and (d) the extensional fault-slip data ($N = 146$) recorded in the pre-Neogene basement of SW Bulgaria. Fault planes are shown as great circles and the slickenlines are shown with solid balls.

the pre-Neogene basement rocks (Fig. 1b). In particular, in the field, the observed frictional grooves or fibrous lineations defining slickenlines (Fleuty, 1974) along differently oriented mesoscale faults (Fig. 3a, b) have been measured and their relative chronology was established on the basis of overprinting relationships as well as the cross-cutting criteria among the faults.

Multiple slips were recorded along several fault surfaces and the determination of the sense of shear has been carried out using S-C cataclastic fabric, offset of stratigraphic markers and microstructures on the fault surface such as R, P shears, T- or comb structures and fibersteps, ripout structures. These markers define the sense of the fault movement and have been widely used as shear sense indicators (Hancock, 1985; Petit, 1987). Due to this, the recorded fault-slip data can be subdivided in contractional and extensional fault-slip data, respectively (Fig. 3c, d).

In addition, the meso-scale faults have been described as normal or reverse faults when the pitch of the slip indicator or rake (r) is $80^\circ \leq r \leq 90^\circ$, as oblique normal or reverse faults when $60^\circ \leq r < 80^\circ$, oblique-slip (contractional or extensional) faults when $30^\circ \leq r < 60^\circ$, oblique strike-slip faults when $10^\circ \leq r < 30^\circ$ and strike-slip faults when $0^\circ \leq r < 10^\circ$.

3.2.1. NE-SW to ENE-WSW faults

The NE-SW to ENE-WSW faults form arrays of faults that dip at medium to high angles toward the NW and in some cases, they have been found to form anastomosing zones with ramp-flat geometries (Fig. 4a, b). The NW-dipping faults cut the main foliation of the basement rocks, as observed in the northern slopes of the Mt. Rila and Mt. Osogovo and south of Kroupnik village and they exhibit three differently orientated groups of slickenlines that are related to three different activations. The older activation corresponds to a left-lateral oblique reverse movement (L1 in Fig. 4c) overprinted by left-lateral oblique normal movement (L2 in Fig. 4c), whereas the youngest one is a right-lateral oblique extensional movement. Along the steeply-dipping faults the youngest slickenlines indicating oblique normal and normal movements are quite scattered.

The NE-SW to ENE-WSW faults that dip at low to intermediate angles toward NW cut the ductile fabric of the rocks (Fig. 4d) and exhibit slickenlines that define normal movements (Fig. 4e). They are more or less parallel to the "Gabrov Dol ductile normal fault" as described by Bonev et al. (1995). However, because they are undulated, some fault surfaces with similar features that belong to these low-angle faults dip at very low-angles toward SW, instead of NW, and because of this they apparently show strike-slip slickenlines (see Fig. 6, A14).

3.2.2. WNW-ESE faults

The WNW-ESE mesoscale faults dip to the NNE at high angles. However, in some outcrops we observe low-angle thrusts dipping NNE (Fig. 4f). The WNW-ESE thrust surfaces show evidence of multiple slip activations, with the slickenlines related to the oldest left-lateral oblique reverse movements being overprinted

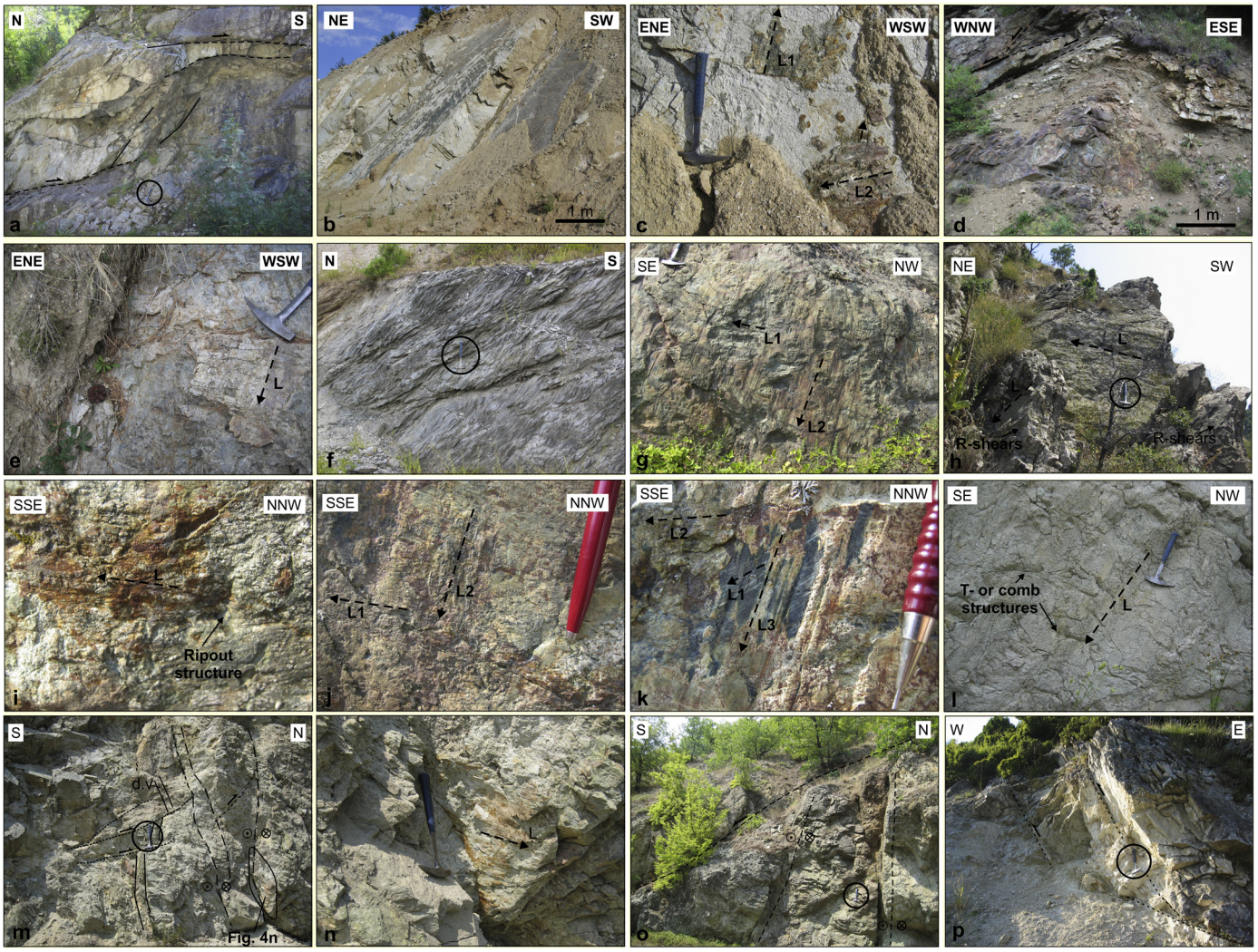

Fig. 4. Field photographs of faults activated during Late Cenozoic times in SW Bulgaria. Location of the photographs is shown with a gray star and a number in Fig. 1b. (a) An anastomosing ENE-WSW trending thrust fault (location 1) revealing ramp-flat geometry in the Osogovo granite, which indicate SSW-directed thrusting on the left-side of the road going parallel to the stream south of the Garliano town (D1 event), (b) a large slickenside-striated fault cutting the exposed Osogovo granite along the road Garliano-Vrattsa (location 2), and (c) the close-up view of the surface of (b), which bears both contractional (L1) and strike-slip (L2) slickenlines. The L1 slickenlines correspond to oblique left-lateral contractional movement (D1 event) and were overprinted by L2 slickenlines which correspond to a left-lateral strike-slip movement (D2 event), (d) an open E-W fold affected by the NE-SW trending extensional faults that dip at low angle toward NW in the northern mountain slopes of Rila Mt. (location 3), (e) close-up view of a NW-dipping low-angle fault in the same region. The dip-slip quartz-fiberlines (L) indicate extensional activation of NE-SW low-angle extensional faults (location 4), (f) an array of WNW-ESE trending repeated thrusts, directed toward the SSW forming S-C fabric within the phyllites of the Frolosh Formation (sensu lato), east of Skrinio village (location 5), (g) a large NNW-SSE fault located on the Bobochevo-Kyustendil road, a few km before Pastouch village (location 6). The almost dip-slip slickenlines (L2) dominate the fault surface and overprint the previously formed strike-slip slickenlines (L1) indicating extensional reactivation of these faults, (h) a large NW-SE fault in the Kroupnik area (location 7). The fault surface is dominated by strike-slip slickenlines (L) and corrugations. The Riedel shears (R-shears) are well developed, indicating a right-lateral sense of movement, (i, j, k) close-up view of the fault surface showed in (g); (i) in this photo the right-lateral strike-slip movement is indicated by the slickenlines (L) and the ripout structures, (j) shows the strike-slip slickenlines (L2) overprinted by dip-slip slickenlines (L3), (k) a similar close-up view showing the dip-slip slickenlines (L3) overprinting the previously formed strike-slip (L2) and oblique strike-slip (L1) slickenlines, (l), close-up view of a NE-dipping fault in the granitoid rocks along the national road Kresna-Krupnik (location 8) on which the right-lateral oblique extensional movement is indicated by the slickenlines (L) and the T- or Comb-structures, (m) low-angle thrusts associated with N-S shortening displacing the vertical thin diabase dykes, which were cut by E-W left-lateral strike-slip faults close to Pastouch village (location 9), (n) is a close-up view of the E-W left-lateral strike-slip fault showing left-lateral strike-slip slickenlines in the same location with (m). Its position is marked in the previous photo (n), (o) a general view of the vertical E-W left-lateral strike-slip faults, which were cut by an extensional NW-SE fault dipping at moderate angles toward SW close to Pastouch village (location 9), (p) NE-dipping reverse faults at the contact between the marbles and the Oligocene sediments (i.e., labeled as $raPg_3^{2-3}$ in Razlog geological map sheet) (location 10). Explanation: Dashed lines indicate the described structures, dashed arrows indicate the direction of different slickenlines L1, L2, . . ., and the relative movement of the missing fault compartment etc., and half-arrow indicates the relative sense of movement along the faults. The large blank circle indicates the position of the hammer.

by those related to the left-lateral contractional strike-slip movements. However, the majority of these faults have been reactivated as extensional faults bearing slickenlines that define right-lateral oblique-slip extensional movements, and more dominantly normal movements with slip trending N-S. The latter are similar with those observed along the faults that bound the Quaternary basins in the region (Tranos et al., 2006) and thus they can be considered as the youngest ones.

3.2.3. NNW-SSE to NW-SE faults

The mesoscale faults that strike NNW-SSE contain steeply-inclined slickenside surfaces that dip toward ENE (Fig. 4g), whereas the NW-SE striking faults dip at high to medium angle either NE or SW. At their majority, they are characterized by multiple slip activations.

More precisely, the kinematics of the NNW-SSE faults is characterized by slickenlines that are related to, from oldest to youngest:

(1) a right-lateral strike-slip movement, which is well defined by Riedel structures and ripout structures (Fig. 4h, i, j, k), and (2) oblique normal movement (Fig. 4l), which is associated with the formation of brecciated gouges. In contrast, the faults that strike WNW-ESE and that display scattered oblique normal and normal movements were formerly activated as left-lateral strike-slip faults.

3.3. Fault cross-cutting relationships

Fault cross-cutting relationship is an issue which needs to be addressed to determine the chronological order among the activated faults. Several outcrops show that:

(1) NE-SW to ENE-WSW left-lateral oblique reverse faults dipping at moderate angles toward NW-NNW have been systematically found associated with the NNW-SSE right-lateral strike-slip faults acting seemingly as transfer faults. However, the latter, in places where they have been reactivated as dip-slip normal faults, cut entirely the former.
(2) The NE-SW to ENE-WSW left-lateral oblique reverse faults and the NNW-SSE right-lateral strike-slip faults were cut by ENE-WSW (sub)vertical left-lateral strike-slip faults (Fig. 4m, n). Moreover, along the NE-SW to ENE-WSW fault surfaces the reverse motions predated left-lateral strike-slip ones.
(3) The ENE-WSW left-lateral strike-slip faults are cut by NW-SE faults that dip at intermediate angles toward the SW (Fig. 4o), in the case the latter have been activated as extensional oblique to normal faults. Several of these NW-SE extensional faults juxtapose Neogene sediments against basement rocks. The ENE-WSW strike-slip faults are also cut by the NNW-SSE to NNE-SSW oblique normal and normal faults.
(4) The NW-SE oblique to normal faults and the NNE-SSW to NE-SW left-lateral oblique extensional faults were cut by the ENE-WSW to WNW-ESE normal faults, with the latter usually bounding Quaternary filling basins and morphological depressions.
(5) The high-angle ENE-WSW to WNW-ESE striking normal faults cut the low-angle ENE-WSW striking faults (Tranos et al., 2006).

4. Methods for kinematic and paleostress analyses

Since the 1970s a variety of methods have been proposed in order to reconstruct paleostress states from field measurements of fault striations on fault planes and their succession (e.g., see Lacombe, 2012; Célérier et al., 2012 for a recent state of the art and a critical discussion of assumptions and limits of paleostress reconstructions). Most of these methods assume that the sampled faults are homogeneous, i.e., slipped independently in a homogeneous stress field and that the recorded slickenlines represent the direction of maximum shear stress on the fault plane. However, it is common in nature for fault-slip data to be heterogeneous, i.e., they result from more than one applied stress tensor.

In general, the methods for analyzing and separating stress tensors from heterogeneous fault-slip data can be roughly grouped into three main procedures (Liesa and Lisle, 2004): manual procedures, semiautomatic procedures that minimize a given parameter, and automatic procedures based on attributes of faults. The manual procedures are based on graphical representations of the results, which are used to differentiate stress tensors. Some of the graphical procedures, such as the Right Dihedra (Angelier and Mechler, 1977) and Right Trihedra (Lisle, 1987, 1988) methods, allow the recognition that data are heterogeneous, but do not allow the definition of the full parameters of the related stress tensors. On the other hand, the graphical y–R diagram method (Simón Gómez, 1986) and its modification by Fry (1992) as well as the methods of Fry (1999) and Yamaji (2000) permit the separation of the stress tensors. In addition, the recently proposed graphical TR method permits the separation of the heterogeneous fault-slip data and the definition of the full parameters of the stress tensors with the aid of a stress inversion method (Tranos, 2012, 2013).

The second category of procedures comprises numerical methods that automatically minimize some parameter, usually the sum of the angular misfits (differences between theoretical striae predicted from some trial tensor and the actual striation), to search for the best tensor to fit the faults and then analyze the remaining non-fitting faults to search for other tensors. Although these inversion methods are automatic, the separation of different stress tensors and therefore the separation of natural field data into homogeneous fault-slip data need to be carried out manually, so that they can rather be considered as semi-automatic procedures for separating stress tensors. Methods that use this approach are those proposed by Etchecopar et al. (1981), Armijo et al. (1982), Angelier (1979, 1984), and Galindo-Zaldívar and González-Lodeiro (1988) amongst others. It is clear, however, that (a) a mixed stress tensor could be defined by these iterations, (b) several fault-slip data could be compatible with more than one calculated stress tensors, and (c) the first iterations contain much more fault-slip data than the succeeding ones and therefore are more robust taking into account the percentage of the fault-slip data included.

In the third category of procedures, an automatic separation of homogeneous data sets is performed from heterogeneous data, but fault-slip data are separated before the inversion process takes place, e.g., the cluster separation procedure proposed by Nemcok and Lisle (1995). In this method, the striation data of each fault are checked for compatibility with a large number of tensors.

The evaluation of the reliability of methods for separating paleostress tensors from heterogeneous fault-slip data by Liesa and Lisle (2004) suggests that attempts to design a fully automatic separation procedure for distinguishing and separating homogeneous data sets from heterogeneous ones will be unsuccessful because the researcher will always be required to take some part in the correct choice of the tensors. In this sense, they consider that additional structural data such as geometrical characteristics of the faults (e.g. conjugate or quasi-conjugate Andersonian systems), stylolites or joints/veins will be very useful for the correct separation of stress tensors from fault-slip data. However, to define real conjugate or quasi-conjugate Andersonian fault systems in a multi-deformed terrain is by itself a very difficult task since this geometry can be apparently the composite result of different faulting events.

For this reason, a different approach to separate the fault-slip data is followed herein and it is based on the use of the contraction (P) and extension (T) kinematic axes (Marrett and Allmendinger, 1990). The idea is that heterogeneous fault slip data can be separated into homogeneous groups by taking into account their kinematic compatibility. The resolved stress tensors from these homogeneous fault slip groups can subsequently be used in order to define the stress regimes that have been applied to the region.

In particular, by subdividing the P and T axes of the fault-slip data in different groups taking into account their orientation, and defining all the possible P–T pairs we can define fault-slip data groups that are characterized by a kinematic compatibility. If the fault-slip data that were included in a P–T group are more than four then they can be used for the determination of a stress tensor with the use of a stress inversion method. The resolved stress tensors from the fault-slip data of these P–T groups are examined taking into account their vertical stress axis (assuming an Andersonian stress regime), the trend of the horizontal stress axis and the stress ellipsoid shape ratio with the goal to evaluate if they define similar stress regimes as those recognized by Tranos et al. (2008). In that case, the resolved stress tensors of the P–T pairs define similar

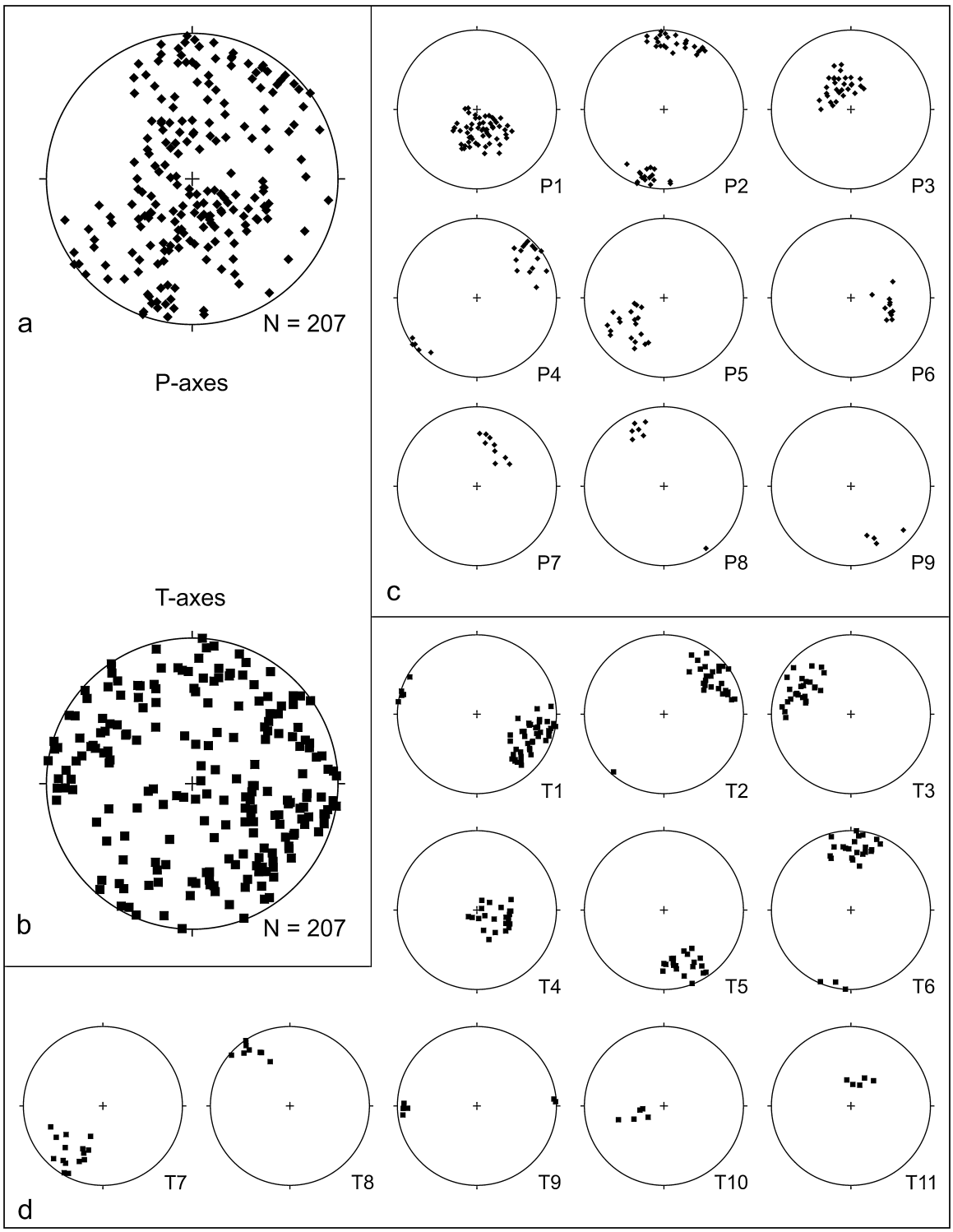

Fig. 5. Stereographic projection (equal area, lower hemisphere) of (a) the P-axes of all fault-slip data, (b) the T-axes of all fault-slip data, (c) and (d) the different P-axes and T-axes groups (labeled P1, . . ., P9 and T1, . . ., T11 respectively) as defined in the present study.

stress regimes then new stress tensors are resolved after merging the fault-slip data belonging to these P–T pairs.

The approach proposed hereinafter, which combines manual (graphical) and semi-automatic (numerical) step-by-step procedure, was applied to the whole fault-slip data population ($N = 207$) recorded in the field. It uses the orientation of the kinematic shortening (P) and extension (T) axis of each fault-slip datum to subdivide the whole fault-slip population into different groups, but not in a manual manner as traditionally used by previous researchers, but in an automatic and consequently in a more objective way. The P–T axes, although familiar to seismologists, are fundamentally kinematic in nature, representing the principal axes of the incremental strain tensor for the fault (Marrett and Allmendinger, 1990). Each pair of axes lies in the 'movement plane' containing the slip vector and the normal to the fault plane and each of them makes an angle of 45° with the slip vector.

The P and T-axes were separately projected in a lower-hemisphere equal area stereonet with the use of the StereoNett

Table 1
The fault-slip data population ($N = 207$) used in this analysis, the trend and plunge of the defined Pi and Ti groups, $i = 1, 2, \ldots$ subgroups. It is also shown with N the number of the fault-slip data included in the P- and T-axes groups as well as the percentage (%) of the whole population each group contains respectively.

$N = 207$	P1 (165-66)	P2(010-00)	P3(330-66)	P4(O53-15)	P5(236-48)	P6(105-54)	P7(024-54)	PS(333-18)	P9(150-36)
N	59	43	30	19	19	11	10	7	4
%	28.5	20.8	14.5	9.2	9.2	5.3	4.8	3.4	1.9

$N = 207$	T1(110-21)	T2(055-21)	T3(294-33)	T4(111-69)	T5(162-30)	T6(010-21)	T7(216-30)	T8(319-15)	T9(261-06)	T10(251-57)	T11(026-69)
N	47	28	26	22	20	24	15	8	6	5	5
%	22.7	13.5	12.6	10.6	9.7	11.6	7.2	3.9	2.9	2.4	2.4

Table 2
A1, A2, . . ., A16 are the PT-PKG defined by the combinations of the P and T axes of Table 1 that include at least four fault-slip data. The included fault-slip data are shown in the brackets.

$N = 207$	P1 (155-66)	P2(010-00)	P3(330-66)	P4(053-15)	P5(236-48)	P6(105-54)	P7(024-54)	P8(333-18)	P9(150-36)
Tl(110-21)	A1(5)	A5(17)	A8(7)	2	A12(10)	0	A14(5)	1	0
T2(O55-21)	A2(15)	1	A3(6)	0	3	0	0	2	1
T3(294-33)	A3(13)	A6(6)	0	3	1	2	0	0	1
T4(111-59)	0	A7(14)	0	2	2	0	0	A16(4)	0
T5(162-30)	1	0	A10(14)	3	1	0	0	0	0
T6(010-21)	A4(21)	0	0	0	1	1	0	0	0
T7(216-30)	0	0	3	1	0	A13(6)	A15(4)	0	1
T8(319-15)	2	0	0	A11(5)	0	1	0	0	0
T9(2S1-O6)	2	3	0	0	0	0	1	0	0
T10(251-57)	0	1	0	3	0	1	0	0	0
T11(026-69)	0	1	0	0	1	0	0	0	1

computer program (Duyster, 2000) (Fig. 5). The P-axes that lie around the highest concentration of the P-axis diagram with a threshold (or cut-off) angle of 30° were picked up and extracted from the initial population forming a P1 group, the mean value of which can be estimated. After the extraction of the P1 poles from the initial population, the same procedure was repeated on the nested diagram of the P-axes in order to define the next P2 group and from this step-by-step repetition we entirely separate the whole population of the P-axes into different groups P*i*, $i = 1, 2, 3, \ldots, n$. This process outlasts until the remaining poles of the P axes could not form a group with more than four poles. We also accomplished the same procedure for the T-axes. More precisely, from the T-axes diagram we separate the T-axes into T*j*, $j = 1, 2, 3, \ldots, n$, until the remaining poles of the T-axes could not form a group with more than four poles. The last limitation relates to the stress space, i.e., at least four differently oriented fault-slip data are needed for the calculation of the stress tensor (Etchecopar et al., 1981).

In our case, nine groups of P-axes describing 97.6% and eleven groups of T-axes describing 99.5% of the whole fault population, respectively (Table 1) have been defined by the aforementioned procedure (Fig. 5). They theoretically describe $9 \times 11 = 99$ different combinations or groups of P*i*T*j* axes (Table 2). However, from all the possible PT combinations, only sixteen, namely herein 'PT-Proper Kinematic Groups' (PT-PKG) contain more than four fault-slip data and therefore only from them a best-fit stress tensor can be calculated (Table 3) with the use of any stress-inversion technique. We use herein for the calculation of the best stress tensor, the Tensor computer program (Delvaux, 1993).

The Tensor computer program as developed by Delvaux (1993) and described by Delvaux and Sperner (2003) defines the best stress tensor of the fault-slip data taking into account the slip sense. It computes the four parameters of the reduced stress tensor, as defined in Angelier (1979, 1991), i.e., the principal stress axes: σ_1 (maximum compression), σ_2 (intermediate compression) and σ_3 (minimum compression) and the stress (ellipsoid shape)

Table 3
The best-fit stress tensor as defined with the Tensor computer program (Delvaux, 1993) of the PiTi combinations that contain more than four fault-slip data (i.e., PT-PKG or PT-Proper Kinematic Groups). n: total population of fault-slip data of group, nt: the number of data used in the stress inversion, σ_1: maximum stress axis, σ_2: intermediate stress axis, σ_3: minimum stress axis, R: stress ratio $(\sigma_2 - \sigma_3)/(\sigma_1 - \sigma_3)$, a°: minimization of deviation angles between observed and predicted slips on fault planes, stress regime as defined by Tranos et al. (2008).

TENSOR	PT_PKG	N	nt	σ_1	σ_2	σ_3	R	V.AKIS	a°	Stress regime D*	Stress regime T*	Rank
T-A1	A1	5	5	233-61	012-21	109-19	0.21	σ_1	5.76	RE	RE-PE	E
T-A2	A2	15	15	161-64	312-22	047-11	0.32	σ_1	9.73	PE	RE-PE	B
T-A3	A3	13	13	190-63	049-13	314-13	0.23	σ_1	3.42	RE	RE-FE	C
T-A4	A4	21	20	176-30	273-01	003-10	0.25	σ_1	3.12	PE	RE-PE	B
T-A5	A5	17	17	011-13	239-70	104-14	0.53	σ_2	13.63	55	55	C
T-A6	A6	6	6	214-12	107-56	311-32	0.5	σ_2	1.5	55	55	D
T-A7	A7	14	14	013-16	277-17	144-67	0.41	σ_3	9.49	PC	PC	C
T-A8	A8COR	4	4	315-45	045-00	135-45	0.43	–	3.05	OBLIQUE	–	E
T-A9	A9	6	6	331-60	149-30	240-01	0.52	σ_1	5.13	PE	PE	D
T-A10	A10COR	11	11	325-72	071-05	162-13	0.35	σ_1	3.19	PE	RE-PE	C
T-A11	All	5	5	045-03	149-76	315-13	0.53	σ_2	7.26	55	55	E
T-A12	A12COR	7	7	310-33	201-00	111-02	0.53	σ_1	11.3	PE	PE	D
T-A13	A13	6	6	094-59	312-25	214-17	0.43	σ_1	7.12	PE	PE	D
T-A14	A14COR	4	4	355-32	233-36	114-33	0.2	–	3.27	OBLIQUE	–	E
T-A15	A15	4	4	044-63	302-06	203-26	0.19	σ_1	2.17	RE	RE-PE	E
T-A16	A16	4	4	354-23	251-24	123-52	0.65	σ_3	3.27	PC	PC-RC	E

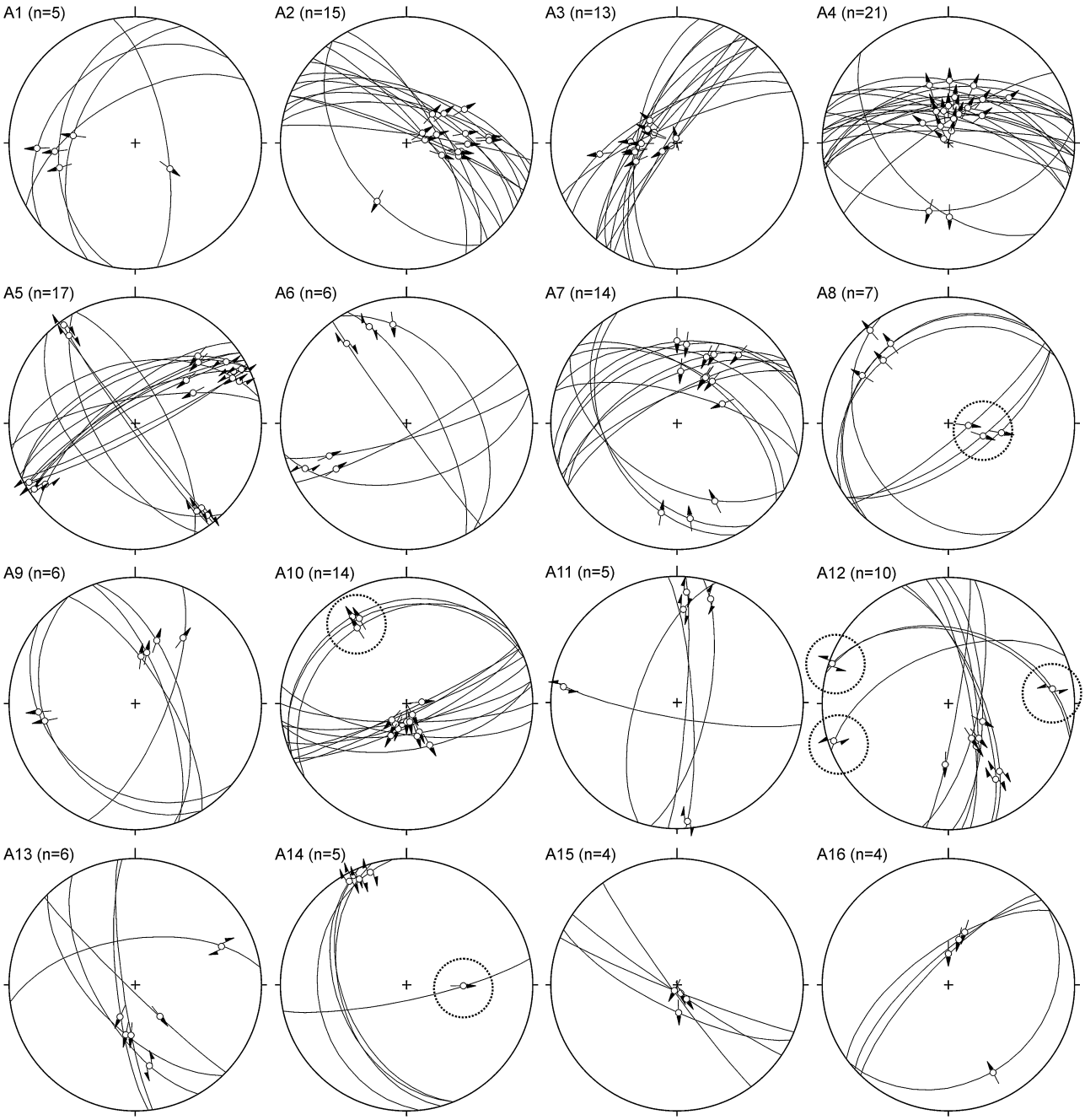

Fig. 6. Stereographic projection (equal area, lower hemisphere) of the PT_PKG groups as defined in SW Bulgaria. Dashed circle indicates the excluded fault slip data due to field observations (see text for an explanation).

ratio $R=(\sigma_2-\sigma_3)/(\sigma_1-\sigma_3)$. The first four parameters are determined using an improved version of the Right Dihedron method of Angelier and Mechler (1977), and step-by-step redefined by the rotational optimization method.

In addition, an important characteristic of the state of stress is the stress regime, which is determined as extensional when σ_1 is vertical, strike-slip when σ_2 is vertical and compressional when σ_3 is vertical and further subdivided upon the stress ratio R (e.g., Delvaux et al., 1997; Tranos et al., 2008).

Prior to the calculation of the stress tensors, the fault-slip data in every PT-PKG (Fig. 6) have to be examined if they satisfy the principal assumption of every stress-inversion method, i.e., that the fault-slip data in the PT-PKG were simultaneously activated. This examination can be done by a careful check with the aforementioned field cross-cutting and overprinting observations. Therefore, a PT-PKG is considered to be acceptable if its fault-slip data do not contradict each other taking into account the above mentioned field criteria. Whenever a PT-PKG contains few fault-slip data that according to the field criteria contradict to each other, the PT-PKG has to be corrected by removing the contradictory fault-slip data that are less in number. In the case, the nested group contains more than four fault-slip data a new group named PT-PKG-COR is taken into account. In turn, if the removed fault-slip data are more than four in number, they can form themselves a new PT-PKG-COR.

In our case, from the sixteen initial PT-PKGs, four groups, i.e., A8, A10, A12 and A14, contain fault-slip data that might not fit to each other taking into account the field observations. In particular, the faults in the A8 and A10 because of the reason 5 of Section 3.3, the faults in the A12 because of the reason 3 of the Section 3.3, and

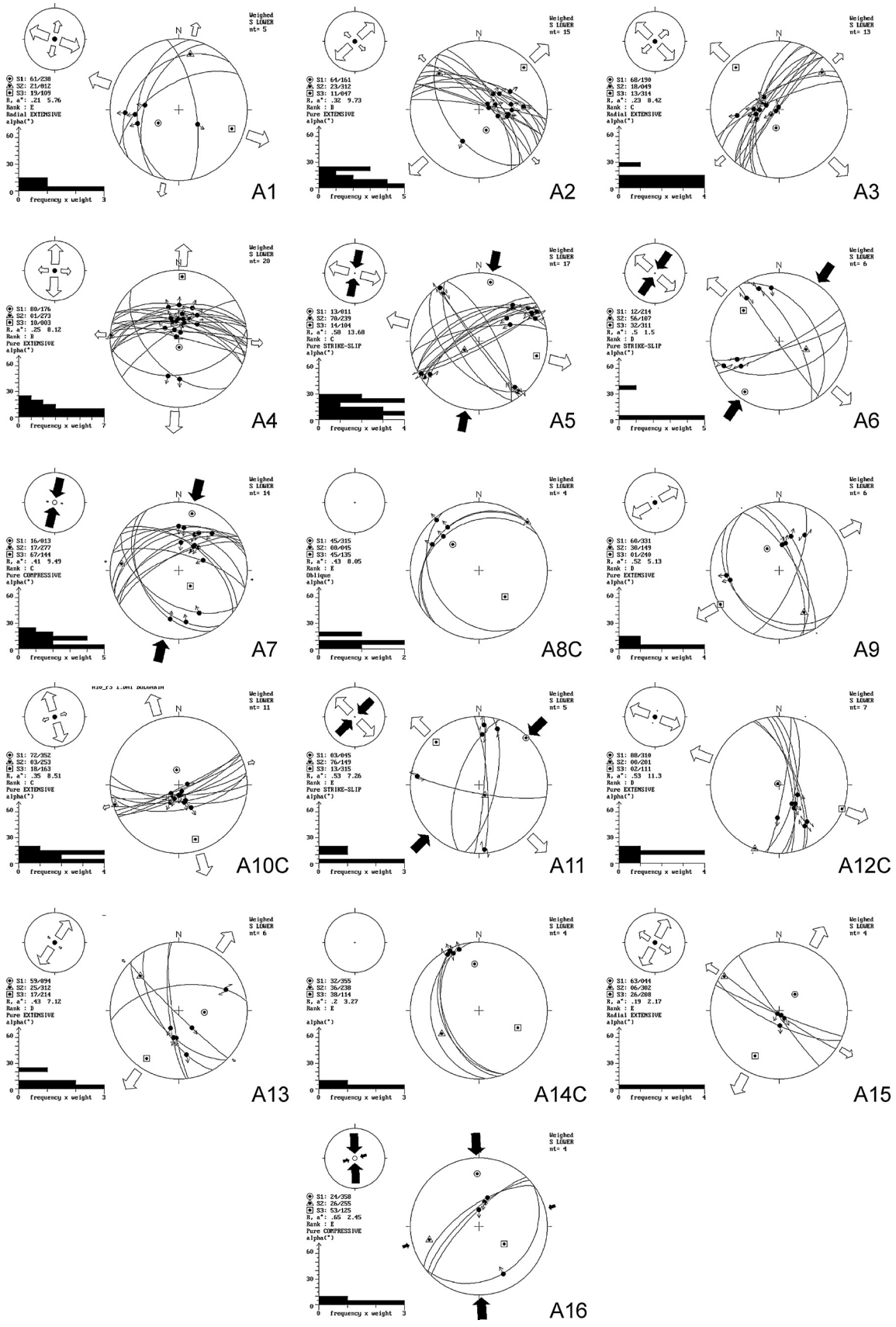

Fig. 7. The best stress tensors of the A1, . . ., A14 PT-PKG of the study area calculated with the use of the Tensor program (Delvaux, 1993). Bar histogram indicates the misfit angle between the theoretical and real slip vector of the fault-slip data and for the accepted solution it is less than 30° for each fault-slip datum and less than 15° in average.

Table 4
The best-fit stress tensor as defined with the Tensor computer program (Delvaux, 1993) of the PT-M_PKG. Symbols as in Table 3.

TENSOR	M_PKG	*N*	nt	σ_1	σ_2	σ_3	*R*	V.AXI5	*a*°	Stress regime D*	Stress regime T*	RANK
T-B1	A7A16	13	13	009-13	274-13	133-67	0.56	σ_3	9.5	PC	PC	C
T-B2	A5A6A11	23	21	026-12	177-76	295-06	0.22	σ_2	11.75	compSS	SS-TRP	B
T-B3	A3CORA14COR	B	3	333-42	232-13	123-45	0.4	–	6.39	OBLIQUE	–	0
T-B4	A1A3A12COR	25	24	207-70	CĈ-zC	05-309	0.16	σ_1	9.97	RE	RE-PE	B
T-B5	A2A9A13A15	31	25	116-73	314-17	223-06	0.13	σ_1	10.39	RE	RE-PE	B
T-B6	A4A10C0R	32	30	103-90	272-00	002-00	0.02	σ_1	3.53	RE	RE	A

the faults in the A14 because the E-W high-angle extensional faults are considered to represent younger activations than the NNW-SSE right-lateral strike-slip faults, especially when the latter are of low-angle dips (Fig. 6).

As a result, new corrected PT-PKG-COR are defined from these which are labeled A8COR, A10COR, A12COR and A14COR (Table 3). Finally, the accepted PT-PKGs are sixteen in number and they gather approximately 70% of the whole population of the fault-slip data. Based on overprinting criteria among the different fault-slip data, the following relative chronological order among the PT-PKGs are established: (1) A2 > A4, (2) A5 > A15, (3) A8COR > A9, (4) A5 > A13, (5) A13 > A4, (6) A11 > A12COR, (7) A7 > A5, (8) A5 > A2, (9) A6 > A2, (10) A5 > A9, with [>] = [older than].

From the sixteen PT-PKGs we subsequently calculate sixteen stress tensors and stress regimes that are labeled T-A1, . . ., T-A16 (Fig. 7; Table 3).

In order to increase the number of the fault-slip data from which a stress tensor is calculated, we further combine the PT-PKGs groups upon the similarities their calculated stress tensors T-A1, . . ., T-A16 present. There are several possible alternative strategies for using the data on pair-wise similarities to decide on the division of the sample into sub-groups or clusters (see Everitt, 1980, pp. 23–58). In our case, the procedure which has been used is the pair-group method of the pair-wise clustering analysis and the Euclidean distribution taking into account parameters of the stress tensors such as: (a) the vertical axis, (b) the stress ratio, and (c) the trend of the horizontal stress axis. It has been accomplished with the PAST software (Hammer et al., 2001) and the clustering results in the following merging cases (Fig. 8): (a) A7 and A16, (b) A5, A6 and A11, (c) A1, A3 and A12COR, (d) A8COR and A14COR, (e) A2, A9, A13 and A15, (f) A4 and A10COR which form the P–T 'Merged Proper Kinematic Groups' (M-PKGs).

The calculated stress tensors from the M-PKGs are the T-B1, T-B2, . . ., T-B6 respectively containing approximately 60% of the whole fault-slip data population. They are fairly considered as acceptable solutions (Fig. 9 and Table 4) taking into account a misfit angle between the theoretical and real slip vector of the fault-slip data less than 30° for each fault-slip datum and less than 15° in average. The T-B1 and T-B2 tensors define a NNE-SSW compressional stress regime with thrusts and strike-slip faults, respectively. The T-B3 and T-B4 stress tensors define a NW-SE extension, but their main difference is that the former activated low-angle faults, whereas the latter activated high-angle faults. However, the T-B3 stress tensor is not well constrained because the fault-slip data do not have a high variability in orientation.

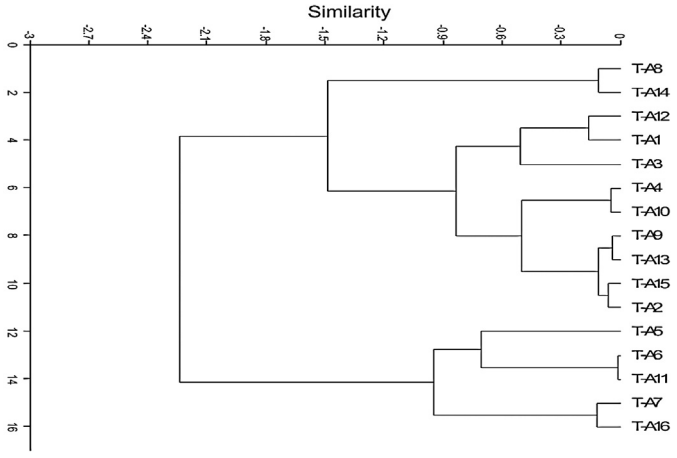

Fig. 8. Division of the T-A1, . . ., T-A16 tensors into sub-groups or clusters using the pair-group method of the pair-wise clustering analysis and the Euclidean distribution as provided by the PAST software (Hammer et al., 2001). The division is based on parameters such as (a) the vertical stress axis, (b) the stress ratio, and (c) the trend of the horizontal stress axis.

Finally, the T-B5 and T-B6 tensors define NE-SW and N-S extension respectively, with the former activating high angle faults striking NW-SE and the latter high angle faults striking E-W.

Although the available tectonostratigraphic criteria are not sufficient to unambiguously constrain the age of the faulting events and related stress tensors, the sequence of faulting could be established from the field cross-cutting and overprinting criteria. As a result, the relative chronological order among the different stress tensors is T-B1 to T-B6 from older to younger.

A next step is to enhance the M-PKGs with the fault-slip data that have not yet been incorporated in the above described procedure. On doing this, we discriminate the latter upon the fault type, e.g., thrusts ($pt \geq 60°$), strike-slip faults ($pt \leq 30°$), oblique-slip extensional faults ($30° \leq pt \leq 60°$), and thus these fault-slip data are included into the different M-PKGs (Table 5). Since there are four different stress tensors, i.e., T-B3, T-B4, T-B5 and T-B6 that define extension, the further subdivision of the extensional faults has to be done using the trend of their T-axis. However, prior to the use of these enhanced groups which are named here 'Enhanced Proper kinematic groups' E-PKGs, we have to exclude from them the faults that according to field criteria do not satisfy the simultaneous assumption.

Table 5
The best-fit stress tensor as defined with the Tensor computer program (Delvaux, 1993) of the PT-E_PKG. Symbols as in Table 3.

TENSOR	E_PKG	*N*	nt	σ_1	σ_2	σ_3	*R*	V. AXIS	*a*°	Stress regime D*	STRESS Regime t*	Rank
T-C1	T-B1+-T	23	23	010-13	275-17	135-63	0.56	$\alpha 3$	9.5	PC	PC	E
T-C2	T-B24-SS	23	23	027-14	166-72	294-11	0.22	$\alpha 2$	11.69	compSS	SS-TRP	D
T-C3	T-B3-HEXT NW	11	11	333-45	234-09	135-44	0.33	-	6.79	OBLIQUE	–	C
T-C4	T-B4-HEXT NW	31	31	204-75	039-15	303-04	0.16	$\alpha 1$	9.34	RE	RE-PE	E
T-C5	T-B5-HEXT NE	31	31	119-73	314-17	223-05	O.2	$\alpha 1$	11.1	RE	RE-PE	E
T-C6	T-B6-i-EXT_N	32	32	223-33	036-01	356-01	0.01	$\alpha 1$	3.97	RE	RE	A

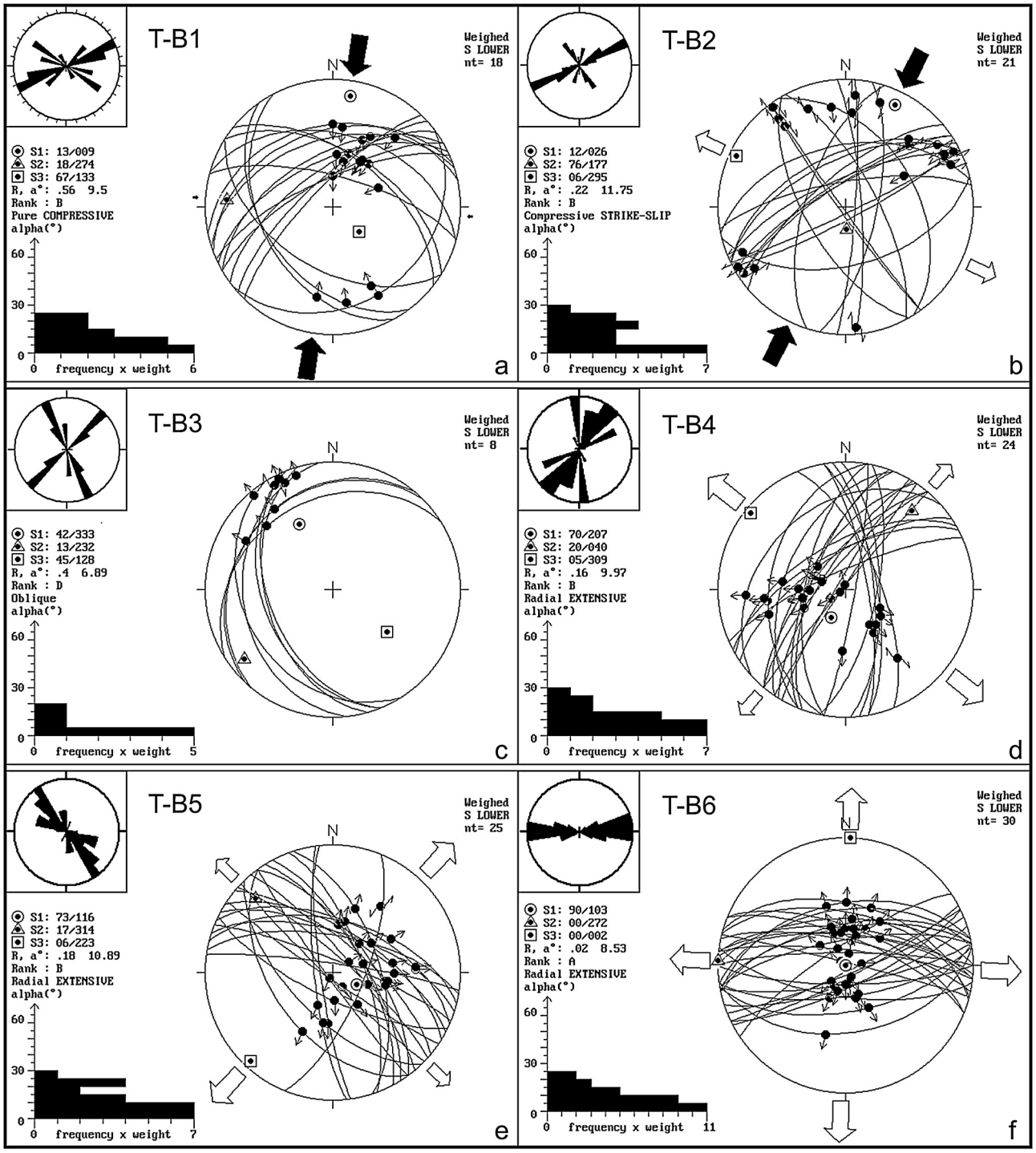

Fig. 9. The best stress tensors of the A1, . . ., A14 PT-M_PKG of the study area calculated with the use of the Tensor program (Delvaux, 1993). Small inset rose-diagram indicates the strike of the faults in each stress inversion solution.

The E-PKGs give tensors that labeled T-C1 to T-C6 (Fig. 10) and in comparison with the T-B1 to T-B6 do not present significant changes in the orientation of the principal stress axes. The total number of the fault-slip data that have been resolved from these tensors are approximately 73% of the field recorded fault-slip data.

Finally, the resulting stress tensors were applied on the whole recorded fault-slip data with the goal to define which other fault-slip data can be dynamically explained by these stress tensors without taking into account their slip tendency as introduced by Morris et al. (1996). This procedure can indicate not only which faults are dynamically compatible with each of the stress tensor, but to which degree a statistically defined best-fit stress tensor can be defined by the application of the stress inversion methods.

The solutions are shown in Fig. 11 and the interesting issue is that all the extensional stress tensors that are characterized by a small stress ellipsoid shape ratio can dynamically activate a

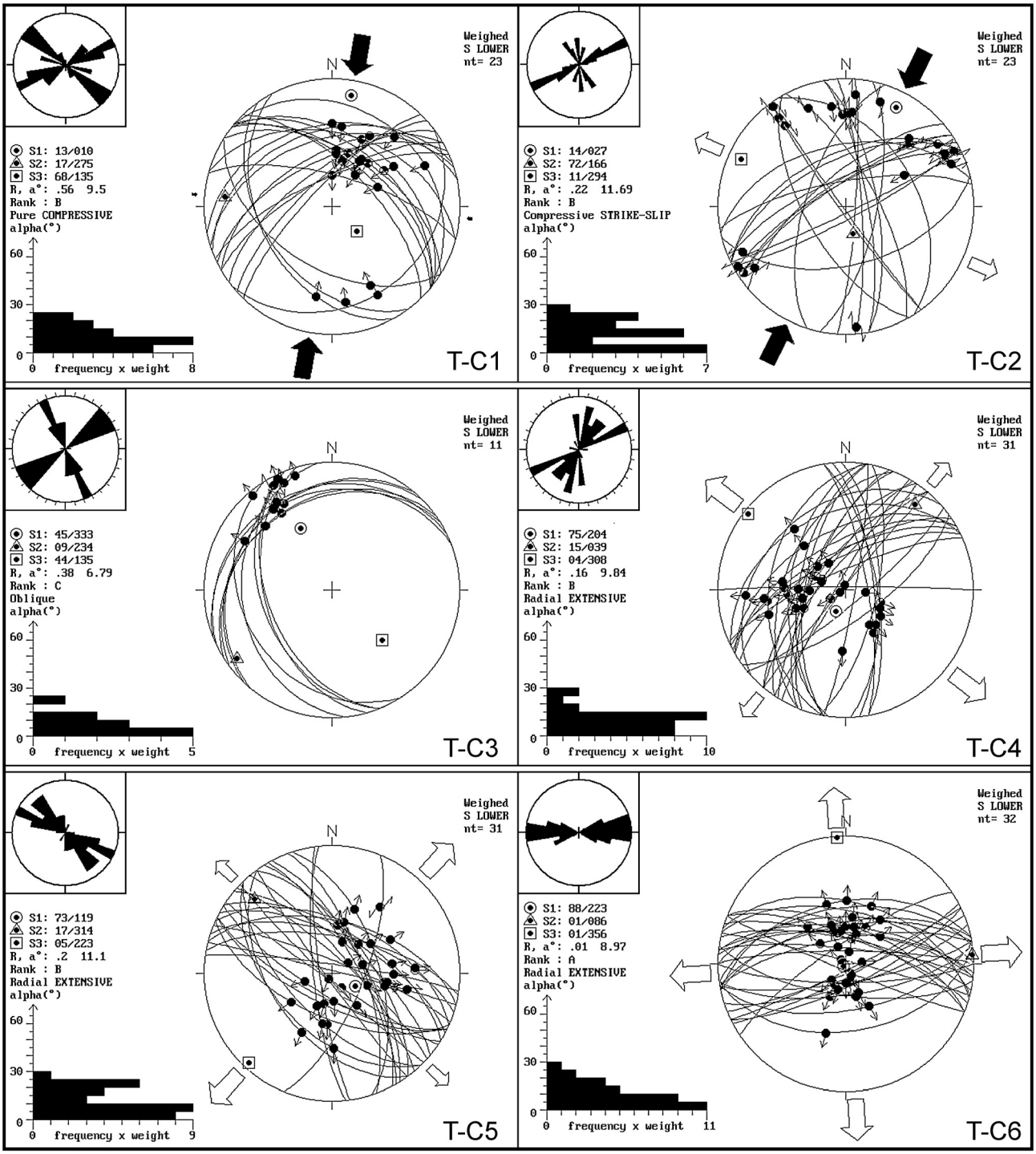

Fig. 10. The best stress tensors of the PT-E_PKG of the study area with the use of the Tensor program (Delvaux, 1993). Small inset rose-diagram indicates the strike of the faults in each stress inversion solution.

very large number of faults. In particular, the application of the two T-C5 and T-C6 tensors to the whole fault population ($N = 207$) (Fig. 11e, f) clearly indicates that the direct application of a stress inversion method on a large number of fault-slip data could not necessarily define the real stress tensor. The reason for this is that the stress inversion method is defining a statistically accepted stress tensor for most of the normal faults and may result in a resolved stress tensor with stress shape ratio close to zero. Indeed, although the least principal stress axes of these two stress tensors trend at different directions, the low value of the stress ellipsoid shape ratio allows switching of the intermediate and least principal stress axes so that both tensors can activate a large number of faults.

5. Results: deformational events and related states of paleostress

The above analysis points to five deformational events namely here D1, D2, D3, D4 and D5, which have deformed the area since the Latest Oligocene.

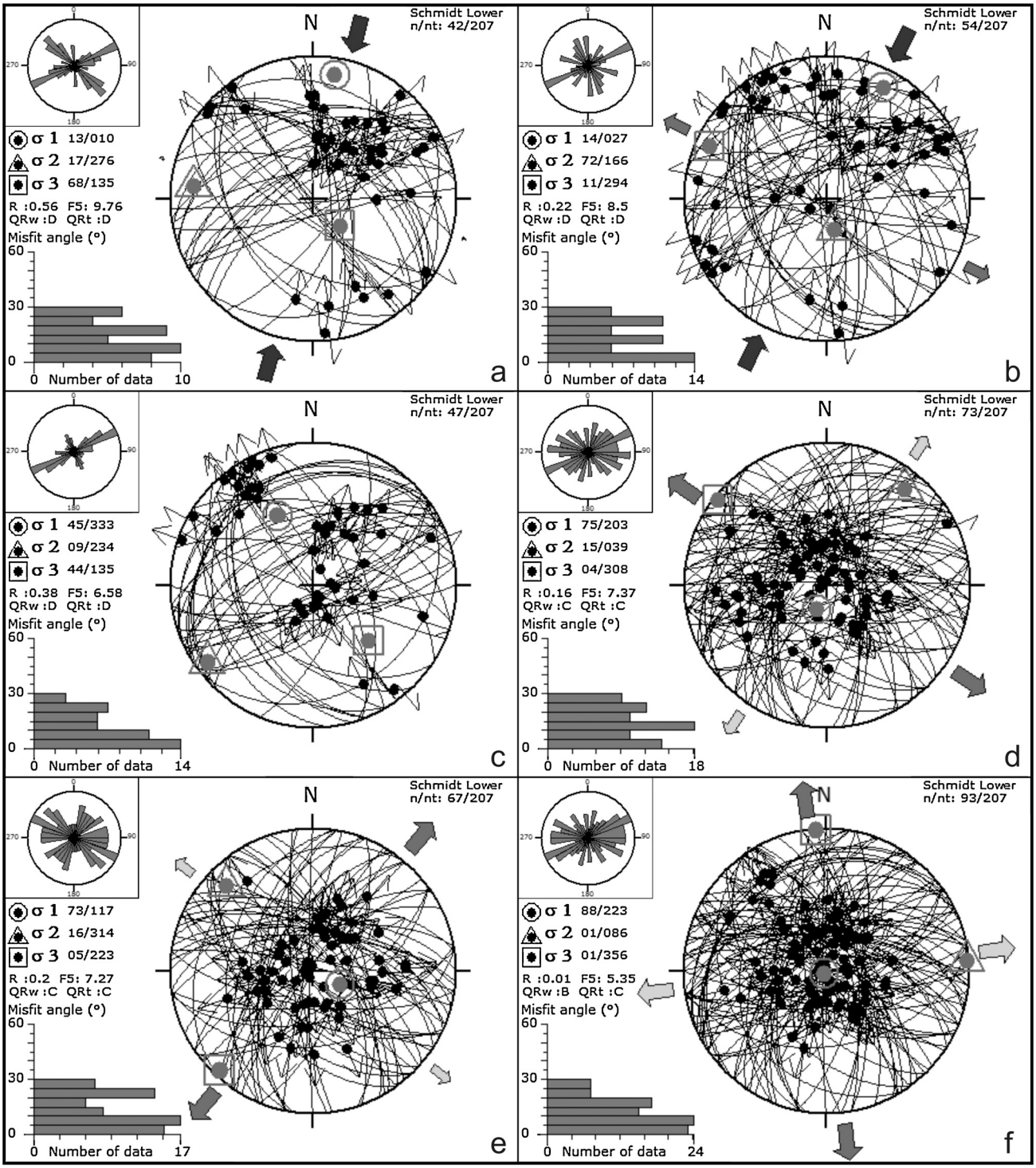

Fig. 11. The application of the PT-E_PKG stress tensors to the whole recorded fault population with the use of the Tensor program (Delvaux, 1993). The application indicates which fault-slip data can be activated by them. (a) T-C1, (b) T-C2, (c) T-C3, (d) T-C4, (e) T-C5 and (f) T-C6. Notice the large number of fault-slip data that can be activated both by T-C5 and T-C6; see text for explanation. Small inset rose-diagram indicates the strike of the faults in each stress inversion solution.

As a result, they can be described as follows:

5.1. D1 (PC) event (Late Oligocene-Earliest Miocene)

This event is the oldest recognized brittle faulting event in the study area. It mainly activated WNW-ESE to NW-SE striking reverse faults to right-lateral oblique faults, and ENE-WSW striking left-lateral oblique-reverse faults (Fig. 10a).

The calculated T-C1 stress tensor has maximum principal stress axis (σ_1) plunging to the N (010°-13°), intermediate principal stress axis (σ_2) plunging gently to the W (275°-17°), least principal stress axis (σ_3) plunging at high angles toward SE (135°-68°) and a stress ratio R equal to 0.56 (Table 5). The R value and the nearly vertical attitude of the σ_3 axis favors a pure compression (PC) stress regime. Strain compatibility (slip in the intersection of the fault surfaces; see Marrett and Allmendinger, 1990) between the differently oriented activated faults is well observed. The latter advocates

that: (a) the majority of the fault-slip data could be attributed to activation of medium to high-dipping lateral ramps formed along with less exposed low-angle frontal ramps directed to SSW, and (b) the SSW transport direction is well constrained by the majority of the fault-slip data the slip vectors of which trend NNE-SSW (~020°). The application of the enhanced stress tensor T-C1 (pure compression) to the whole fault population (Fig. 11a) shows that some NW-SE to N-S trending and NE-SW trending faults can also be activated as right-lateral strike-slip faults and left-lateral strike-slip faults, respectively. D1 event is constrained as old as Late Oligocene because D1-structures affect the Osogovo granite (Fig. 4a, b, c), the crystallization of which was dated radiometrically in Middle Oligocene (30.6 ± 1.6 Ma, Graf, 2001). In addition, such a compression is shown in the geological map-sheets of Blagoevgrad (Marinova and Zagorchev, 1990a) and Kyustendil (Zagorchev, 1991) to affect the Eocene-Oligocene sediments exposed in the region between the Kyunstendil and Dupnitsa towns. In particular, these clastic rocks are folded dipping either toward NE or SW with common angles of 30° and at several places their contact with the crystalline rocks of Frolosh Formation or Struma Diorites is a thrust bringing the latter rocks over the Oligocene sediments as indicated by drilling project (see Fig. 5 of Zagorchev, 1992). At the contact between the marbles and the Oligocene sediments (location 10 shown in Fig. 1b) such reverse fault surfaces (Fig. 4p) dipping toward the NE, i.e., the basement side have been observed. If we consider that the basin inversion dated by Graf (2001) at 25 Ma was the result of the D1 event, then the D1 event onsets in the Latest Oligocene. This conclusion is also supported by the fact that similar end of sedimentation, erosion and basin inversion that was related with a compression of the region has been also reported for the same period in the Eastern Thrace basin and Saros Gulf (Saner, 1985; Görür and Okay, 1996; Turgut and Eseller, 2000) as well as in the North Aegean Trough (Roussos, 1994; Tranos, 2009; Kilias et al., 2013).

The D1 structures do not affect the Neogene sediments (Zagorchev, 1992; Tranos et al., 2008) and therefore D1 event predates the onset of Sarmatian sedimentation. Further south, in Central Macedonia of Northern Greece and North Aegean similar N-S compression has been reported to affect the basement rocks in Late Oligocene-Early Miocene times (Tranos, 1998, 2009, 2011; Tranos et al., 1999, 2009; Georgiadis et al., 2007) under a transpressional stress regime. In terms of strain, where the orientation of shortening or extension axis and the geometry and kinematics of the structures is taken into consideration the deformation can be described as pure shear dominated oblique contraction taking into account that the σ_1 axis is close to the shortening axis.

5.2. D2 (SS-TRP) event (Early-Middle Miocene)

D2 event activated faults striking NE-ENE as left-lateral strike-slip faults and faults striking NNW-N as right-lateral strike-slip faults (Fig. 10b), facilitating the quasi-conjugate faulting. The calculated T-C2 stress tensor has a vertical σ_2 axis and a stress ratio $R = 0.22$ that suggests a strike-slip-transpression (SS-TRP) stress regime. The σ_1 axis of the stress regime is horizontal trending NNE-SSW (027°) and the least principal stress axis (σ_3) trends NW-SE. Thrusting does not outlast this stress regime. The application of the T-C2 stress tensor to the whole fault population is shown in (Fig. 11b). The geometry and kinematics of the structures suggests that the deformation in terms of strain can be described as wrench dominated oblique contraction.

Tranos et al. (2008) constrained this event in Early-Middle Miocene, and more precisely before the Pontian since it affects sedimentary rocks as young as those of the Meotian Chernichevo Formation of the Simitli basin. Similar age has been constrained farther southwards in the Strymon basin (Tranos, 2011).

5.3. D3 (PE and PE-RE) event (Middle-Late Miocene)

Two different stress tensors T-C3 and T-C4 with a common least principal stress axis (σ_3) trending along NW-SE define the D3 deformational event.

The first tensor (T-C3) (Fig. 10c) with stress ratio $R = 0.38$, and the greatest and least principal stress axes in oblique position, activated NW-dipping low-angle extensional faults and SW-dipping low-angle right-lateral strike-slip faults. The oblique position of the principal stress axes departs from the Andersonian mode of faulting (Anderson, 1951), but this results from the fact that the used fault-slip data are not kinematically independent on each other. Because of this, the resolved stress tensor T-C3 could not be considered as a reliable one.

In broader sense, these fault surfaces are similar in orientation with the large extensional shear zone of the "Gabrov Dol ductile normal fault" as the latter has been mapped by Bonev et al. (1995) and has been interpreted to result by a post-Middle Cretaceous to pre-Middle Oligocene extension. The mechanical feasibility of the activation of low-angle extensional faults is a matter of debate (see Collettini, 2011; Lacombe et al., 2013). These authors argue that although geological observations indicate that the low-angle faults are common in extensional environments the particular conditions that can explain both their initiation and movement cannot be easily met in nature. Low-angle extensional faults trending NE-SW have been reported in Northern Greece to affect the metamorphic rocks, but also the Oligocene molasse-type sediments due to an NW-SE extension dated Middle-Late Miocene (Tranos, 2009, 2011). In any case, the small number of the D3 low-angle faults in SW Bulgaria along with their vague dating, perhaps, implies that these low-angle fault surfaces represent a limited reactivation of the Early Tertiary detachment faults.

On the other hand, assuming that the later T-C4 tensor (Fig. 10d) has stress axes orientations that satisfy the Andersonian mode of faulting and that its intermediate principal stress axis σ_2 is in common position (subhorizontal trending NE-SW) with that of T-C3 tensor implies that they were initially high-angle faults of the T-C3 tensor and that their present attitude might result from their tilting of about 40° around the intermediate σ_2 axis.

The T-C4 tensor with $R = 0.16$ suggests a radial-pure extension (RE-PE) stress regime and it activates high-angle faults, the strike of which varies from N-S to NE-SW. Similar structures (i.e., D3 structures) in the basinal sedimentary rocks of the Simitli basin and the Strymon basin in Northern Greece have been attributed to a syn-Meotian-earliest Pontian deformation event (Tranos et al., 2008; Tranos, 2011).

In addition, the application of the T-C3 and T-C4 stress tensors to the whole fault population is shown in Fig. 11c, d respectively. The NW-SE trending faults with gentle dips to the SW and strike-slip kinematics are dynamically compatible with the T-C3 tensor; a fact that fits well with that has been defined for them in the field, i.e., functioning as apparent strike-slip faults. Although, a quite large number of faults with a high dispersion in orientation is dynamically compatible with the T-C4 stress tensor showing that the inherited fault pattern played a significant role on the faulting of the region during this event, the strike rose- diagrams (Fig. 11c, d) indicate that the NE-SW to ENE-WSW faults are dynamically the most admissible for activation.

5.4. D4 (PE-RE) event (Late Miocene-Pliocene)

D4 event caused the activation of faults with strike that varies from WNW-ESE to NNW-SSE as oblique normal faults to normal

faults. The more different the fault strike from the NW-SE direction, the more oblique the displacements on them. The calculated T-C5 stress tensor (Fig. 10e) has σ_1 vertical, σ_3 horizontal trending NE-SW (043°) and a stress ratio $R = 0.2$ so as to define a radial to pure extension (PE-RE) stress regime similar with the RE-PE stress regime of the previous D3 deformational event, except the fact that the least principal stress axis (σ_3) trends normal to the previous one. Nonetheless, this reveals the difficulty one has to discriminate these faults only by following blindly the stress-inversion techniques. This event is dated in Late Miocene-Pliocene times by interrelating the geometry and kinematics of these faults with those that bound and developed the Strouma graben system. The application of the T-C5 stress tensor to the whole fault population is shown in (Fig. 11e) and indicates that dynamically compatible with it are mainly the faults trending WNW-ESE, NW-SE and NE-SW and less the faults trending ENE-WSW.

5.5. D5 (RE) event (Lower Pleistocene-Present)

The D5 event is defined by the T-C6 stress tensor (Fig. 11) which has a vertical σ_1 axis, σ_3 horizontal trending N-S and stress ratio $R = 0.01$. As a result, it is a truly radial extension (RE) stress regime activating mainly high-angle normal faults the strike of which could vary about 30° around E-W. In addition, the application of the T-C6 stress tensor to the whole fault population is shown in (Fig. 11e) and indicates that the most compatible faults with this tensor are the ENE-WSW.

The fact that these faults (1) cut the NW-SE fabric made up by the NW-SE normal faults and the similarly trending basins and (2) bound E-W trending basins that filled up with Quaternary sediments constrains their age in Quaternary times. These faults (Fig. 2a) have been already described as seismically active faults related to the N-S extensional contemporary stress field that prevails in SW Bulgaria (Tranos et al., 2006), and is responsible for several earthquakes over the last century (e.g., Meyer et al., 2002, 2007; Kotzev et al., 2006; Papadimitriou et al., 2006, etc.). In particular, the P–B–T axes defined with the aid of Win_Tensor software from the focal mechanisms of the earthquakes shown in Fig. 2b (black rhomps; data from Kotzev et al., 2006) clearly yield an N-S extension for the contemporary stress regime in the host region; a fact that fits well with the World stress map (Heidbach et al., 2010).

6. Discussion of results and regional implications

The Tertiary deformation history of the hinterland part of the Hellenic and Balkan orogen has been challenged by several geoscientists that have proposed different evolutionary schemes to explain the pervasive exhumation tectonics that followed large-scale thrusting (see Burg, 2012 and reference therein). Of great importance in this history is the recognition of several gneiss domes limited by detachment faults which have been interpreted as metamorphic core complexes due to a Cenozoic extension. In particular, such core complexes and detachment faults have been recognized in the Kraishte zone and Western Rhodope Massif of West Bulgaria (Bonev et al., 1995; Graf, 2001; Kounov et al., 2004; Peychev et al., 2012), in Eastern Rhodope Massif of Thrace (Mposkos and Krohe, 2000; Bonev et al., 2006) and in the Southern Rhodope Massif of central Macedonia (Dinter and Royden, 1993; Sokoutis et al., 1993).

Based on the above mentioned studies the hinterland part of the Hellenic and Balkan orogen is usually considered as having undergone continuous extension from the latest Cretaceous until today. It is important to mention that these studies in their majority focused either on defining the geometry and kinematics of the gneiss domes by studying mainly the ductile deformation in their internal part or on the detachment faults that were considered to play a significant role on the exhumation of these gneiss domes.

However, the studies in the Bulgarian domain rather suggest that the deeper levels of continental crust were exhumed and gneiss domes were formed in response to syn-orogenic extension. This extension started in Late Cretaceous but did not outlast the Oligocene times: evidence are provided by the deposition of post-detachment Oligocene shallow-marine sediments and by the rocks of the accompanying widespread magmatic activity that cut across or sealed the detachment faults (Bonev et al., 2006; Georgiev et al., 2010). On the other hand, the studies in the Greek domain that mainly dealt with the Southern Rhodope metamorphic core complex are more controversial and suggest that this core complex was formed due to a NE-SW extension that started either in Miocene times (Dinter and Royden, 1993; Dinter, 1998; Wawrzenitz and Krohe, 1998; Tranos, 2009, 2011) or in Eocene-Oligocene times (Kilias and Mountrakis, 1990; Kilias et al., 1999; Burchfiel et al., 2000, 2003; Kounov et al., 2004; Brun and Sokoutis, 2007). It is worth mentioning that there are significant controversies among the studies, especially those dealing with the period of activation of the detachment faults. For example, Burchfiel et al. (2003) argue for an Eocene-Oligocene onset of extension on the basis of the study of the Mesta half-graben and its detachment and considering that this fault is part of a larger extensional system that also includes the Miocene Strymon Valley detachment fault. In contrast, Georgiev et al. (2010) and Peychev et al. (2012) argue that the Mesta detachment was activated in Eocene-Oligocene times but not later and thus it has no structural relationship with the Strymon Valley detachment fault. According to these authors the Mesta detachment was cut by the Strymon Valley detachment in Miocene. Georgiev et al. (2010) placed without any further clue a phase of relative tectonic quiescence between the Early Tertiary syn-orogenic and the Middle-Late Miocene post-orogenic extension. On the other hand, relatively older studies, i.e., Moskovski (1968a,b, 1969), Moskovski and Harkovska (1973), as well as more recent ones suggest that a contraction event affected the hinterland in Late Oligocene-Early Miocene times (Zagorchev, 1992; Tranos et al., 2008, 2009; Tranos, 2011). An intriguing issue is that the activation of the Nestos Shear Zone in the Rhodope Massif until approximately 32–33 Ma clearly indicates that a persistent syn-metamorphic thrusting dominated the Hellenic hinterland until the Early Oligocene (Gautier et al., 2010; Georgiev et al., 2010; Nagel et al., 2011). Furthermore, studies focused on brittle deformation and the definition of the paleostresses in the hinterland region since the Oligocene always indicate a much more complex brittle deformation which is associated with thrusts and strike-slip faults during the Late Oligocene (e.g., Zagorchev, 1992; Koukouvelas and Doutsos, 1990; Tranos, 1998, 2004, 2009, 2011; Georgiadis et al., 2007; Tranos et al., 2008, 2009). Tranos et al. (2008) and Tranos (2009, 2011) explained this deformation in the hinterland as a late-collisional transpression driven by the Apulia-Eurasia collision. It is also interesting that Kilias et al. (1999) who suggested a continuous extension since the Eocene-Oligocene, now working with faulting deformation in the hinterland argue for a transpressional stress regime during the Oligocene-Miocene times (Kilias et al., 2013).

It is clear that the peripheral basins over the Rhodope Massif metamorphic core complex have been inverted and compressed during the Latest Oligocene-Early Miocene times. However, one can assume this as a result of the uplift and exhumation of the metamorphic core complex of the Rhodope Massif under a thoroughgoing extension as already proposed by several authors. However, the metamorphic core complex of Rhodope at its largest part has been already exhumed by that time. Furthermore, although, the thrusts in the hinterland are not as many in number and as large in size possibly due to the younger brittle deformational events, they have been reported not only on the periphery of the core complex, but

in the metamorphic rocks of the Rhodope, as well. In particular, thrusts have been reported for the same period in the rocks of the Serbo-Macedonian massif (Kilias et al., 1999; Tranos, 1998, 2011) and the Southern Rhodope metamorphic core complex, i.e., the Sidironero Unit (Koukouvelas and Doutsos, 1990) and the underlying Pangeon Unit (Kilias and Mountrakis, 1990; Tranos et al., 2008, 2009).

Another critical issue is that the separation between the D1 and D2 events that both share similar trends of σ_1 axis might not be realistic, if one assumes that the thrusts of the D1 event could have been formed in restraining bends of the large strike-slip faults of the D2 event. Although the available tectonostratigraphic criteria are not as plenty as to robustly resolve this issue, the fact that strike-slip displacements, but not reverse displacements, have been reported for faults affecting the Early-Middle Miocene sediments of Simitli basin (Tranos et al., 2008) and Strymon basin (Tranos, 2011) advocates for the separation of the D1 and D2 events. Besides, this separation is based on the field cross-cutting and overprinting criteria that suggest that the strike-slip displacements are younger than the oblique reverse/reverse displacements on the faults activated by the D1 and D2 events. Because of this, the D1 and D2 events are here considered as two-end member deformation stages with the D1 event (PC) having evolved progressively to D2 event (SS-TRP); a fact that indicates the waning of the compressional stresses during time.

On the other hand, the fact that the recent paleostress analysis of Kounov et al. (2011) could not define any faulting deformation from the Middle Miocene onwards raises questions about their proposal chronological order of the stress regimes that governed the hinterland region, since the stress regimes fail to explain (a) the large basins in the region, such as the Strouma-Sandanski, Simitli, Doupnitsa and Bansko-Razlog, that are filled up with Neogene and Quaternary sediments, (b) the recent topography and main physiographic features, and (c) the recent seismicity of the region that includes large destructive earthquakes, e.g., Krupnik-Kresna, SW Bulgaria, earthquake of April 1904, with a reported magnitude of Ms7.8 (Christoskov and Grigorova, 1968), that indicate that faulting has been the dominant deformational process in the area since the Neogene (Tranos et al., 2006, 2008).

Anyway, the most crucial issue for the better understanding of the Tertiary deformation that gave rise to the present-day architecture of the Hellenic hinterland and the exhumation processes is whether the late-orogenic processes, dominating the area just after the Eocene orogenic stacking, can be separated or not from the post-orogenic processes having started from Late Miocene onwards as suggested by the formation of the Neogene basins (Lyberis, 1985; Pavlides and Kilias, 1987; Mercier et al., 1989; Zagorchev, 1992; Tranos, 1998, 2011).

The present paper indicates that the fault pattern of SW Bulgaria includes various faults that have been activated since the Late Oligocene due to the D1, D2, D3, D4 and D5 deformational events and therefore that the Late Tertiary deformation history of the area is not as simple as implied by the models of orogenic collapse and metamorphic core complex development.

More precisely, this history includes deformational events that could be better described in terms of strain as pure shear dominated oblique contraction during the Late Oligocene-Earliest Miocene (D1 event) to wrench dominated oblique contraction during the Early-Middle Miocene (D2 event). The D3 event postdates the D2 event during the Middle-Late Miocene, and although short in time, corresponds to the first extension defined by the fault-slip data of the area. The least principal stress axis (σ_3) during the D3 event trends NW-SE, as the least principal stress axis of the D2 event does; a fact that points to a NW-SE orogen-parallel extension.

As a result, the Late Oligocene-Middle-Late Miocene faulting deformation of SW Bulgaria described by D1, D2, and D3 events and therefore the deformation of the hinterland part, is here explained as the result of the late orogenic processes driven by the collision of the Apulia plate with the Moesian platform of Eurasia (Tranos, 2004; Tranos et al., 2008). Similar deformation has been recognized southwards in Central Macedonia (Tranos, 1998), along the boundary of the Serbo-Macedonian massif with the CRBTS and Axios zone (Tranos et al., 1999; Georgiadis et al., 2007) as well as in the Eastern Balkans (Doglioni et al., 1996; Sinclair et al., 1997). A critical age constraint on the late-collisional deformation is provided by the Philippi granitoid that intruded the Pangeon Unit in the Greek Rhodope massif around 30 Ma (Tranos et al., 2009). According to these authors this granitoid has been deformed by the N-S to NNE-SSW compression that gave rise to the NE-SW folding that dominates the Pangeon Unit and later on by the activation of strike-slip faults similar with those of the present D2 event.

Another important issue is that the D2 event clearly indicates that the deformation of the hinterland part of the Hellenic orogen was not driven by an orthogonal collision between the Apulia and Eurasia plates, but rather by a right-lateral oblique collision, while the orogen-parallel extension (D3 event) represents the final stage of this late collisional deformation stage.

The D4 event, as defined here, is dated in Late Miocene-Pliocene and is the only extensional stress regime with the least principal stress axis oriented NE-SW. As a result, D4 event suggests that the orogen-orthogonal extension was firstly established from the Late Miocene onwards and because of this the fault-bounded basins of the hinterland have their long axis along the NW-SE orientation (Pavlides and Mountrakis, 1987; Mercier et al., 1989; Pavlides and Kilias, 1987; Zagorchev, 1992; Tranos, 1998). Among these basins, the NW-SE striking narrow Strouma-Sandanski graben and the Strumon basin along the Strouma River in SW Bulgaria and Northern Greece respectively are closer to our study (Zagorchev, 1992; Tranos et al., 2008; Tranos, 2011).

D5 is the latest event that activates faults the strike of which varies at about 30° around E-W, but mainly the ENE-WSW; a fact that is supported by the morphotectonic features of the region. Besides, several of these faults bound the WNW-ESE, E-W and ENE-WSW trending, km-long, narrow basins, such as the WNW-ESE trending Bansko-Razlog basin, the ENE-WSW Kyustendil-Garliano basin and the E-W Petritsi basin. This event is considered to have dominated the area from Early Pleistocene onwards, modifying all the previous structures and giving rise to the extended Pleistocene and Holocene proluvial sedimentation along the ENE-WSW and WNW-ESE trending mountain fronts as well as the alluvial sedimentation along the rivers.

As a result, we propose the following tectonic scenario:

The collision between the Apulia and Eurasia plates took place in Tertiary times, forming the alpine Dinaric-Hellenic belt in the Balkan Peninsula. The Apulia front as outlined at present by the NNW-SSE-striking alpine Dinaric-Hellenic belt includes advancing and retreating parts and consequently the final configuration of the alpine mountain belt is rather complex. In particular, a significant control on the final shape of the alpine mountain chains in the Balkan domain appears to be the retreating plate boundaries that gave rise to the ENE-drifted Carpathian and SSW-drifted Hellenic mountain fronts. Of equal importance, however, is the Moesia platform that stands as the Eurasia promontory in the central eastern Balkan territory and around which the Romanian Carpathians and Balkan mountain chains have been formed. The crustal mass between the Moesia platform and the alpine Dinaric-Hellenic belt that strikes WNW-ESE in the Oligocene times (Fig. 12a) were intensely squeezed and because of this, it was forced to extrude laterally around the Moesia and in the region of South Balkan toward the Aegean Sea.

The late stage of this process took place in Latest Oligocene-Earliest Miocene with compressional stresses giving rise to

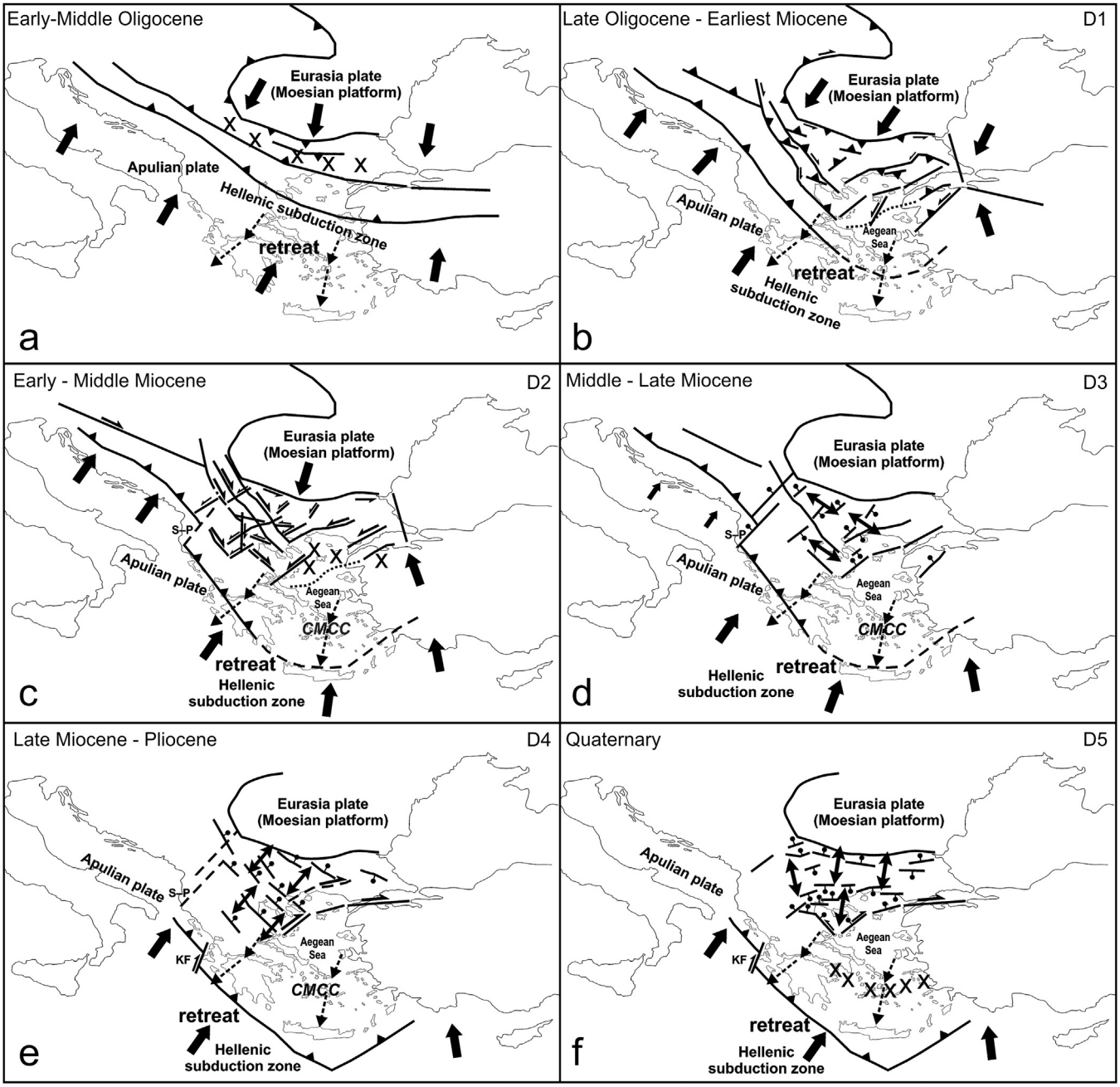

Fig. 12. Evolutionary schematic maps depicting the faulting deformation of the Balkan Peninsula due to the Apulia-Eurasia plate convergence since the Oligocene. (a) General situation of the Apulian-Eurasian convergent boundary in Early-Middle Oligocene, (b) Late Oligocene-Earliest Miocene. The late collision stage between the Eurasia promontory, i.e., Moesian platform and the Apulia continent is dominated by thrusting deformation until the Earliest Miocene (D1 event) giving rise to the extrusion of the crust toward the SE, i.e., the Aegean Sea, (c) Early-Middle Miocene. The extrusion toward the Aegean Sea took place with a wrench-dominated oblique contraction. The NNW-SSE and NE-SW trending faults behave as right-lateral and left-lateral strike-slip faults, (d) Middle-Late Miocene. (e) Late Miocene-Pliocene. (f) Quaternary-Present. Compressional stresses are shown with one-side solid arrows. Extensional stresses are shown with two-side solid arrows. Dashed arrows indicate the direction of the retreat of the Hellenic subduction zone; Balls on the hanging wall of extensional faults, triangles on the hanging wall of contractional faults; strike-slip displacement or component with half arrows. S-P: Scutari-Pec tectonic line, KF: Kephallonia transform fault, CMCC: Cyclades Metamorphic Core Complex, xxx: magmatic activity.

thrusting along WNW-ESE faults (D1 event, Fig. 12b). The lateral extrusion occurred in Early-Middle Miocene with steeply dipping NW-SE to NNW-SSE and NE-SW faults activated as right-lateral and left-lateral strike-slip faults, respectively, under a wrench dominated oblique contraction (D2 event) (Fig. 12c). In particular, the NNW-SSE trending right-lateral strike-slip faults like the Strouma Lineament were among the westernmost boundaries that accommodated the extrusion toward the SSE, whereas the NE-SW and the WNW-ESE trending D2 structures stand as large, discontinuous, indent-linked, left-lateral strike-slip faults similar to those referred to in the Eastern Balkans (Doglioni et al., 1996; Sinclair et al., 1997) and southerly in the Central Macedonia and North Aegean Sea (Tranos, 1998, 2009, 2011). It is worth mentioning that the subduction retreat of the Hellenic orogen (Le Pichon and Angelier, 1981; Royden, 1993; Kilias et al., 2002; Jolivet et al., 2013) that caused the bend of the orogenic Alpine front, the formation of the arcuate shape of the Hellenides and the formation of the Cyclades metamorphic core complexes (Jolivet et al., 2010) between the Adriatic and Minor Asian regions facilitated the extrusion processes by providing the available space in the Aegean Sea. In addition, we

interpret the Scutari-Pec line as a structure that gave rise to the re-adjustment of the Apulian front against this retreating. Due to this retreat, the boundary of the internal Hellenides with the Hellenic hinterland became arcuate getting a NNW-SSE trend from the Former Yugoslavia domain in the north to the Chalkidiki peninsula of Northern Greece in the south and an ENE-WSW trend from the Chalkidiki peninsula toward the NE (Fig. 12b). This bending of the boundary provided the available space for the formation of the Rhodope metamorphic core complex (Tranos, 2009). This in accordance with the synchronous initiation of the two metamorphic core complexes in Late Oligocene-early Eocene times as considered by Gautier et al. (1999) and Jolivet et al. (2004).

The extrusion process ended in the Middle-Late Miocene when the wrench dominated oblique contraction ceased and the stress regime that subjected to the region was an orogen-parallel extension (D3 event). The latter includes the (re)activation of high-angle and low-angle extensional (detachment) faults that strike NE-SW to ENE-WSW, i.e., normal to the extrusion direction as well as the development of several NE–SW-striking transtensional depocenters, such as the Simitli basin (Tranos et al., 2008) and the larger Sporades basin in the North Aegean Sea (Tranos, 2009). Because of this, this extension can be considered as reflecting the along-transport relaxation of the extruded crust.

From the Late Miocene onwards the brittle deformation of SW Bulgaria as described by D4 (Fig. 12e) and D5 events (Fig. 12f) has similar features, with that of inner Greek domain and the Aegean crust, and seems to be related to the back-arc extension of the present-day Hellenic subduction zone and to the ongoing retreat of the later (Le Pichon and Angelier, 1981). However, a remarkable difference is that during the D4 event (NE-SW extension) the basins were not extended in SW Bulgaria as intensely as in Northern Greece. In addition, that in the Bulgarian domain the least principal stress axis (σ_3) of the D5 event as defined here fits well with that defined in Northern Greece (Mountrakis et al., 2006; Tranos et al., 2006) activating the ENE-WSW faults as oblique normal to normal faults suggests that the large dextral strike-slip displacements of the ENE-WSW faults along the North Aegean Trough (as revealed by the modern earthquakes) even they are in connection with the North Anatolian fault should be restricted to the narrow damage zone of the North Aegean Trough.

It is worth mentioning that the above-described evolution that relates to late-collisional processes during the Late Oligocene-Miocene period fits well with the transpression deformation described more northwards in the Romanian Carpathians by Linzer et al. (1998) for the same period.

At a regional scale, the fact that the D4 and D5 deformational events have been interpreted as a back-arc deformation relating to the retreat of the Hellenic subduction is consistent with the subduction retreat modeling studies of Schellart and Moresi (2013), Meyer and Schellart (2013) and Duarte et al. (2013). The latter have shown that back-arc deformation can occur at very large distances to the interior of the overriding plate (i.e., at distances of 800 km and more from the trench). Moreover, Schellart and Moresi (2013) have indicated that the size of the subduction slab that is retreating plays a significant role on the type of the back-arc deformation of the overriding plate, with the back-arc extension to be facilitated in small sized and moving faster subduction zones than in large in size subduction zones that move slower and which give rise to back-arc contraction. Our tectonic scenario seems to be supported well by these results. In particular, the Eocene collision between Apulia and Eurasia plates refers to a large size subduction zone as traced by the Alpine mountain chain that includes the Dinarides, Albanides, Hellenides and Taurides. Consequently, the late-collisional transpression that dominates the hinterland during the Late Oligocene-Middle Miocene, i.e., simultaneously with the collisional processes in the more external parts of the Hellenides and Dinarides, possibly represent a back-arc contraction due to this large size subduction slab. On the contrary, since the Late Miocene the differential retreat of the subduction zone aided by the large Scutari-Pec and Kefalonia transform faults gave rise to the compartmentalization of the subduction zone and the formation of the smaller in size Hellenic subduction zone. The Hellenic subduction zone retreats in faster rates than the rest boundaries of the Apulia-Eurasia plates and because of this a widespread back-arc extensional deformation dominates the overriding plate even at very large distances from the trench such as in SW Bulgaria.

Our vision on the deformation history of the hinterland between the Dinaric-Hellenic and the Balkan orogens since the Late Cretaceous includes that this hinterland part was (1) a back-arc area in the interior of the Balkan orogen from Late Cretaceous to Early Tertiary times, (2) a volcanic arc related with the subduction and delamination processes between Apulia and Eurasia plates during the Eocene-Oligocene times (see also Pamić et al., 2002), and (3) a back-arc area in the interior of the Hellenic subduction zone since the Miocene when the volcanic activity shifted more southwards to the North Aegean Sea.

7. Concluding remarks

The present paper indicates that the Late Tertiary deformation history of SW Bulgaria and in broader sense of the hinterland area is not as simple as implied by existing models of orogenic collapse and metamorphic core complexes. In contrast, the fault pattern of SW Bulgaria includes various faults that have been activated since the Late Oligocene during D1, D2, D3, D4 and D5 deformational events. D1 is a Late Oligocene-Early Miocene transpression deformation associated with NNE-SSW contraction (D1 event), D2 is an Early-Middle Miocene transpression to strike-slip deformation associated with NNE-SSW contraction and WNW-ESE extension, D3 is a Middle-Late Miocene NW-SE to WNW-ESE extension, D4 is a Late Miocene-Pliocene NE-SW trending extension and D5 is a Quaternary-Present N-S trending extension. The first three events are related to the late-collisional process between the Apulia and Eurasia plates that took place during the Late Oligocene-Middle Miocene describing a pure shear dominated oblique contraction (D1) to wrench dominated oblique contraction (D2) and an orogen-parallel extension (D3), respectively. The next events, D4 and D5 are considered as reflecting back-arc deformation of the overriding plate due to the retreat of the Hellenic subduction zone.

Furthermore, this study proposes a new tectonic evolutionary scenario for the South Balkan region since the Oligocene.

On a methodological point of view, in the present analysis the separation of the fault-slip data on the basis of their kinematic compatibility (i.e., fault-slip data with similar kinematic P and T axes are grouped) is accomplished this in a semi-automatic way. In addition, the resolved stress tensors from these fault-slip groups have been merged by taking into account their vertical stress axis and stress ellipsoid shape ratio, instead of testing a large number of stress tensors as done in the grid methods. The approach herein also permits us to distinguish stress tensors, the parameters of which are quite close to each other and which otherwise could form a mixed stress tensor.

At a regional scale, the present paper demonstrates that during the latest collisional stages of the Hellenic orogen, transpressional tectonics associated with lateral extrusion prevailed in its hinterland, mainly because this hinterland has been located between advancing and retreating plate boundaries. Based on the subduction retreat modeling of Schellart and Moresi (2013), it can be tentatively proposed that the late-collisional transpression governing the hinterland during the Late Oligocene-Middle Miocene times may reflect back-arc contraction related to a large sized and slow

moving retreating plate boundary between Apulia and Eurasia, whereas the widespread extension of the overriding plate since the Late Miocene could be explained as back-arc deformation driven by trench retreat processes of a small size Hellenic subduction zone.

Acknowledgments

Early drafts of this manuscript have been benefited from the reviews of Demosthenis Mountrakis and Vagelis Kakouros. Boyko Ranguelov and Dragomir Gospodinov are sincerely appreciated for their assistance in accomplishing the fieldwork in Bulgaria. Vladislav Kachev and the excellent driver Liubomir Blagov are thanked for their assistance in the field. Vassilis Karakostas is thoroughly acknowledged for his support and association. Daemian Delvaux and Alexandre Kounov are thanked for their review that improved the quality of the manuscript. Last, but not least the editorial assistance by Wouter Pieter Schellart is greatly appreciated.

References

Anderson, E.M., 1951. The Dynamics of Faulting, 2nd ed. Oliver and Boyd, Edinburgh, pp. 206.
Angelier, J., 1979. Determination of the mean principal directions of stresses for a given fault population. Tectonophysics 56, T17–T26.
Angelier, J., 1984. Tectonic analysis of fault-slip data sets. Journal Geophysical Research 89, 5848–5953.
Angelier, J., 1991. Inversion directe et recherché 4-D; comparaison physique et mathétique de deux methods de determination de tenseurs des paléocontraintes en tectonique de failles. Comptes Rendus de l'Académie des Sciences de Paris 312 (II), 1213–1218.
Angelier, J., Mechler, P., 1977. Sur une méthode graphique de recherché des contraintes principales également utilisable en tectonique et en séismologie: la méthode des dièdres droits. Bulletin de la Societe Geologique de France 7, 1309–1318.
Armijo, R., Carey, E., Cisternas, A., 1982. The inverse problem in microtectonics and the separation of tectonic phases. Tectonophysics 82, 145–160.
Bakalov, P.G., Zelev, V.J., 1996. Lithostratigraphy of the Neogene-Villafranchian sediments of the Kjustendil graben. Review of the Bulgarian Geological Society 57 (1), 75–82.
Bonchev, E., 1958. Über die tektonische Ausbildung der Kraistiden (Kraistiden Lineament). Geologie 7, 409–419.
Bonev, K., Ivanov, Z., Ricou, L.-E., 1995. Dénudation tectonique au toit du noyau métamorphique rhodopien-macédonien: la faille normale ductile de Gabrov Dol (Bulgarie). Bulletin of Geological Society of France 166 (1), 49–58.
Bonev, N., Burg, J.P., Ivanov, Z., 2006. Mesozoic–Tertiary structural evolution of an extensional gneiss dome—the Kesebir–Kardamos dome, Eastern Rhodope (Bulgaria–Greece). International Journal Earth Sciences 95, 318–340.
Brun, J.P., Sokoutis, D., 2007. Kinematics of the Southern Rhodope Core Complex (North Greece). International Journal Earth Sciences 96 (6), 1079–1099.
Burg, J.P., 2012. Rhodope: from Mesozoic convergence to Cenozoic extension. Review of petro-structural data in the geochronological frame. In: E. Skourtsos and G.S. Lister (Eds.), The Geology of Greece. Journal of the Virtual Explorer 42 (Electronic Edition, ISSN 1441-8142, paper 1).
Burchfiel, B.C., Nakov, R., Tzankov, T., Royden, L.H., 2000. Cenozoic extension in Bulgaria and Northern Greece: the northern part of the Aegean extensional regime. In: Bozkurt, E., Winchester, J.A., Piper, J.D.A. (Eds.), Tectonics and Magmatism in Turkey and the Surrounding Area. Geological Society, London, pp. 325–352 (Special Publications, 173).
Burchfiel, B.C., Nakov, R., Tzankov, T., 2003. Evidence from the Mesta half-graben, SW Bulgaria, for the Late Eocene beginning of Aegean extension in the Central Balkan Peninsula. Tectonophysics 375, 61–75.
Célérier, B., Etchecopar, A., Bergerat, F., Vergely, P., Arthaud, F., Laurent, P., 2012. Inferring stress from faulting: from early concepts to inverse methods. Tectonophysics 581, 206–219.
Christoskov, L., Grigorova, E., 1968. Energetic and space–time characteristics of the destructive earthquakes in Bulgaria after 1900. Bulletin d'Institut de Geophysique XII, 9–107.
Collettini, C., 2011. The mechanical paradox of low-angle normal faults: current understanding and open questions. Tectonophysics 510, 253–268, http://dx.doi.org/10.1016/j.tecto.2011.07.015.
Delvaux, D., 1993. The TENSOR program for paleostress reconstruction: examples from the east African and the Baikal rift zones. Terra Nova 5 (1), 216.
Delvaux, D., 2011. Version 3.0 and above of the Win-Tensor Program, Available at: http://users.skynet.be/damien.delvaux/Tensor/tensor-index.html
Delvaux, D., Moeys, R., Stapel, G., Petit, C., Levi, K., Miroshnichenko, A., Ruzhich, V., San'kovet, V., 1997. Paleostress reconstructions and geodynamics of the Baikal region, Central Asia. Part II: genozoic tectonic and fault kinematics. Tectonophysics 282 (1–4), 1–38.
Delvaux, D., Sperner, B., 2003. Stress tensor inversion from fault kinematic indicators and focal mechanism data: the TENSOR program. In: Nieuwland, D. (Ed.), New Insights into Structural Interpretation and Modelling. Geological Society, London, pp. 75–100 (Special Publications 212).
Dimitriadis, S., Kondopoulou, D., Atzemoglou, A., 1998. Dextral rotations and tectonomagmatic evolution of the southern Rhodope and adjacent regions (Greece). Tectonophysics 299, 159–173.
Dinter, D.A., Royden, L., 1993. Late Cenozoic extension in northeastern Greece: Strymon Valley detachment system and Rhodope metamorphic core complex. Geology 21, 45–48.
Dinter, D.A., 1998. Late Cenozoic extension of the Alpine collisional orogen, northeastern Greece: origin of the north Aegean basin. Geological Society of America Bulletin 110, 1208–1230.
Doglioni, C., Busatta, C., Bolis, G., Marianini, L., Zanella, M., 1996. Structural evolution of the eastern Balkans (Bulgaria). Marine and Petroleum Geology 13 (2), 225–251.
Duarte, J.C., Schellart, W.P., Cruden, A.R., 2013. Three-dimensional dynamic laboratory models of subduction with an overriding plate and variable interplate rheology. Geophysical Journal International 195, 47–66.
Duyster, J.D., 2000. StereoNett, vers. 2.4, http://homepage. ruhr-uni-bochum.de/Johannes.P.Duyester/Stereo/Stereo1.htm
Etchecopar, A., Vasseur, G., Daignieres, M., 1981. An inverse problem in microtectonics for the determination of stress tensors from fault striation analysis. Journal of Structural Geology 3, 51–65.
Everitt, B.S., 1980. Cluster Analysis, second ed. Heineman Educational Books, London.
Fleuty, M.J., 1974. Slickensides and slickenlines. Geological Magazine 112, 319–322.
Fry, N., 1992. Stress ratio determination from striated faults: a spherical plot for cases of near vertical principal stress. Journal of Structural Geology 14, 1121–1131.
Fry, N., 1999. Striated faults: visual appreciation of their constraint on possible paleostress tensors. Journal of Structural Geology 21, 7–22.
Galindo-Zaldívar, J., González-Lodeiro, F., 1988. Faulting phase differentiation by means of computer search on a grid pattern. Annales Tectonicae 2, 90–97.
Gautier, P., Brun, J.P., Moriceau, R., Sokoutis, D., Martinod, J., Jolivet, L., 1999. Timing, kinematics and cause of Aegean extension: a scenario based on a comparison with simple analogue experiments. Tectonophysics 315, 31–72.
Gautier, P., Gerdjikov, I., Ruffet, G., Bosse, V., Cherneva, Z., Pitra, P., Hallot, E., Persistent synmetamorphic thrusting in the Rhodope until 33 Ma: evidence from the Nestos Shear Zone and implications for Aegean geodynamics 2010. XIX Congress of the Carpathian-Balkan Geological Association, Geologica Balkanica , Thessaloniki, Greece, 23–6 September 2010, pp. 122–123.
Georgiadis, G.A., Tranos, M.D., Mountrakis, D.M., 2007. Late- and post-Alpine tectonic evolution of the southern part of the Athos peninsula, northern Greece. Bulletin of the Geological Society of Greece 40, 309–320.
Georgiev, N., Pleuger, J., Froitzheim, N., Stoyan, S., Jahn-Awe, S., Nagel, T.J., 2010. Separate Eocene–Early Oligocene and Miocene stages of extension and core complex formation in the Western Rhodopes, Mesta Basin, and Pirin Mountains (Bulgaria). Tectonophysics 487, 59–84.
Görür, N., Okay, A.I., 1996. Origin of the Thrace Basin, NW Turkey. Geological Rundschau 85, 662–668.
Graf, J., (Ph.D. thesis) 2001. Alpine tectonics in western Bulgaria: Cretaceous compression of the Kraište region and Cenozoic exhumation of the crystalline Osogovo-Lisec Complex. Swiss Federal Institute of Technology, Zürich.
Hancock, P.L., 1985. Brittle microtectonics: principles and practice. Journal of Structural Geology 7, 437–457.
Hammer, Ø., Harper, D.A.T., Ryan, P.D., 2001. PAST: paleontological statistics software package for education and data analysis. Palaeontologia Electronica 4 (1), 9 http://palaeo-electronica.org/2001_1/past/issue1_01.htm
Harkovska, A., Pecskay, Z., 1997. The tertiary magmatism in Ruen magmato-tectonic zone (W Bulgaria)—a comparison of new K-Ar ages and geological data. In: Boev, B., Serafimovski, T. (Eds.), Magmatism, Metamorphism and Metallogeny of the Vardar Zone and the Serbo-Macedonian Massif. Faculty of Mining and Geology, Štip-Dojran, FYROM, pp. 137–142.
Harland, W.B., 1971. Tectonic transpression in Caledonian Spitsbergen. Geological Magnetism 108, 27–42.
Heidbach, O., Tingayd, M., Barth, A., Reineckere, J., Kurfeß, D., Müller, B., 2010. Global crustal stress pattern based on the World Stress Map database release 2008. Tectonophysics 482 (1–4), 3–15.
Jolivet, L., Brun, J.P., 2010. Cenozoic geodynamic evolution of the Aegean region. International Journal of Earth Sciences 99, 109–138, http://dx.doi.org/10.1007/s00531-008-0366-4.
Jolivet, L., Lecomte, E., Huet, B., Denèle, Y., Lacombe, O., Labrousse, L., Le Pourhiet, L., Mehl, C., 2010. The north cycladic detachment system. Earth and Planetary Science Letters 289, 87–104, http://dx.doi.org/10.1016/j.epsl.2009.10.032.
Jolivet, L., Faccenna, C., Huet, B., Labrousse, L., Le Pourhiet, L., Lacombe, O., Lecomte, E., Denèle, Y., Burov, E., Brun, J.P., Gueydan, F., Philippon, M., Paul, A., Salaün, G., Karabulut, H., Piromallo, C., Monié, P., Okay, A.I., Oberhänsli, R., Pourteau, A., Augier, R., Gadenne, L., Driussi, O., Bozkurt, E., 2013. Aegean tectonics: strain localisation, slab tearing and trench retreat. Tectonophysics 597–598, 1–33, http://dx.doi.org/10.1016/j.tecto.2012.06.011.
Jolivet, L., Rimmelé, G., Oberhänsli, R., Goffé, B., Candan, O., 2004. Correlation of syn-orogenic tectonic and metamorphic events in the Cyclades, the Lycian Nappes and the Menderes massif, geodynamic implications. Bulletin of the Geological Society of France 175 (3), 217–238.
Kahle, H.G., Cocard, M., Peter, Y., Geiger, A., Reilinger, R., Barka, A., Veis, G., 2000. GPS-derived strain rate field within the boundary zones of the Eurasian, African, and Arabian Plates. Journal of Geophysical Research 105 (B10), 23353–23370.

Kilias, A., Mountrakis, D., 1990. Kinematics of the crystalline sequences in the western Rhodope massif. Geologica Rhodopica 2, 100–116.
Kilias, A., Falalakis, G., Mountrakis, D., 1999. Cretaceous-Tertiary structures and kinematics of the Serbo-Macedonian metamorphic rocks and their relation to the exhumation of the Hellenic Hinterland (Macedonia, Greece). International Journal of Earth Sciences 88, 513–531.
Kilias, A., Falalakis, G., Sfeikos, A., Papadimitriou, E., Vamvaka, A., Gkarlaouni, Ch., 2013. The Thrace basin in the Rhodope province of NE Greece—a tertiary supradetachment basin and its geodynamic implications. Tectonophysics 595–596, 90–105.
Kilias, A., Mountrakis, D., 1998. Tertiary extension of the Rhodope massif associated with granite emplacement (Northern Greece). Acta Vulcanologica 10, 331–337.
Kilias, A.A., Tranos, M.D., Orozco, M., Alonso-Chaves, F.M., Soto, J.I., 2002. Extensional collapse of the Hellenides: a review. Revista Societa Geologica España 15 (3–4), 129–139.
Kiratzi, A., 2010. The 24 May 2009 Mw5.2 earthquake sequence near Lake Doirani (FYROM-Greek borders): focal mechanisms and slip model using empirical source time functions inversion. Tectonophysics 490, 115–122.
Kockel, F., Walther, H., 1965. Die Strimonlinie als Grenze zwischen Serbo-Mazedonischem und Rila-Rhodope Massiv in Ost Mazedonien. Geologisches Jahrbuch 83, 575–602.
Kojumdgieva, E., Nikolov, I., Nedjalkov, P., Busev, A., 1982. Stratigraphy of the Neogene in Sandanski Graben. Geologica Balkanica 12 (3), 69–81.
Kolokotroni, C.N., Dixon, J.E., 1991. The origin and emplacement of the Vrondou granite, NE Greece. Bulletin of the Geological Society Greece 25, 469–483.
Kotzev, V., Nakov, R., Georgiev, Tz., Burchfiel, B.C., King, R.W., 2006. Crustal motion and strain accumulation in western Bulgaria. Tectonophysics 413, 127–145.
Koukouvelas, I., Doutsos, Th., 1990. Tectonic stages along a traverse cross cutting the Rhodopian zone (Greece). Geologische Rundschau 79 (3), 753–776.
Kounov, A., Seward, D., Bernoulli, D., Burg, J.-P., Ivanov, Z., 2004. Thermotectonic evolution of an extensional dome: the Cenozoic Osogovo-Lisets core complex (Kraishte zone, western Bulgaria). International Journal of Earth Sciences 93, 1008–1024.
Kounov, A., Seward, D., Burg, J.-P., Bernoulli, D., Ivanov, Z., Handler, R., 2010. Geochronological and structural constraints on the Cretaceous thermotectonic evolution of the Kraishte zone (Western Bulgaria). Tectonics 29, TC2002, http://dx.doi.org/10.1029/2009TC002509.
Kounov, A., Burg, J.-P., Bernoulli, D., Seward, D., Ivanov, Z., Dimov, D., Gerdjikov, I., 2011. Paleostress analysis of Cenozoic faulting in the Kraishte area, SW Bulgaria. Journal of Structural Geology 33, 859–874.
Lacombe, O., 2012. Do fault slip data inversions actually yield "paleostresses" that can be compared with contemporary stresses? A critical discussion. Comptes Rendus Geoscience 344, 159–173, http://dx.doi.org/10.1016/j.crte.2012.01.006.
Lacombe, O., Jolivet, L., Le Pourhiet, L., Lecomte, E., Mehl, C., 2013. Initiation, geometry and mechanics of brittle faulting in exhuming metamorphic rocks: insights from the northern Cycladic Islands (Aegean, Greece). Bulletin de la Société Géologique de France 184 (4–5), 389–409 (Special Issue Faults, stresses and mechanics of the upper crust: a tribute to Jacques Angelier).
Le Pichon, X., Angelier, J., 1981. The Aegean Sea. Philosophical Transactions of the Royal Society A 300, 357–372.
Liesa, C.L., Lisle, R.J., 2004. Reliability of methods to separate stress tensors from heterogeneous fault-slip data. Journal of Structural Geology 26, 559–572.
Linzer, H.G., Frisch, W., Zweigel, P., Girbacea, R., Hann, H.P., Moser, F., 1998. Kinematic evolution of the Romanian Carpathians. Tectonophysics 297, 133–156.
Lisle, R.J., 1987. Principal stress orientations from faults: an additional constraint. Annales Tectonicae 1, 2155–2158.
Lisle, R.J., 1988. ROMSA: a basic program for paleostress analysis using fault-striation data. Computers & Geosciences 14 (2), 255–259.
Lyberis, N., 1985. Tectonic evolution of the North Aegean trough. In: Dixon, J.E., Robertson, A.H.F. (Eds.), The Geological Evolution of the Eastern Mediterranean. Geological Society, London, pp. 709–725 (Spec. Publ. 17).
Marinova, R., Zagorchev, I., 1990a. Geological map of the People's Republic of Bulgaria, 1:100 000 series, Blagoevgrad Sheet. Committee of Geology, Sofia.
Marinova, R., Zagorchev, I., 1990b. Geological map of the People's Republic of Bulgaria, 1:100 000 series, Razlog Sheet. Committee of Geology, Sofia.
Marrett, R., Allmendinger, R.W., 1990. Kinematic analysis of fault-slip data. Journal of Structural Geology 12, 973–986.
Marrett, R., Peacock, D.C.P., 1999. Strain and stress. Journal of Structural Geology 21, 1057–1063.
McClusky, S., Balassanian, S., Barka, A., Demir, C., Erginav, S., Georgiev, I., Gurkan, O., Hamburger, M., Hurst, K., Kahle, H., Kastens, K., Kekelidze, G., King, R., Kotzev, V., Lenk, O., Mahmoud, S., Mishin, A., Nadarya, M., Ouzounis, A., Paradissis, D., Peter, Y., Prilepin, M., Reilinger, R., Sanli, I., Seeger, H., Tealeb, A., Toksoz, M.N., Veis, G., 2000. Global Positioning System constraints on plate kinematics and dynamics in the eastern Mediterranean and Caucasus. Journal Geophysical Research 105, 5695–5719.
Mercier, J.-L., Simeakis, K., Sorel, D., Vergely, P., 1989. Extensional tectonic regimes in the Aegean basins during the Cenozoic. Basin Research 2, 49–71.
Meyer, B., Armijo, R., Dimitrov, D., 2002. Active faulting in SW Bulgaria: possible surface rupture of the 1904 Strouma earthquakes. Geophysical Journal International 148, 246–255.
Meyer, B., Sebrier, M., Dimitrov, D., 2007. Rare destructive earthquakes in Europe: the 1904 Bulgaria event case. Earth and Planetary Science Letters 253, 485–496.
Meyer, C., Schellart, W.P., 2013. Three-dimensional dynamic models of subducting plate-overriding plate-upper mantle interaction. Journal of Geophysical Research 118, 775–790, http://dx.doi.org/10.1002/jgrb.50078.
Morris, A.P., Ferrill, D.A., Henderson, D.B., 1996. Slip tendency and fault reactivation. Geology 24, 275–278.
Moskovski, S., 1968a. On the fault-fold paragenesis of some Paleogenic grabens in the Kraishtid structural zone. In: Geological Institute of BAN and the Committee of Geology, Jubilee Geological Volume, pp. 147–155 (in Bulgarian, with English abstract).
Moskovski, S., 1968b. Tectonic of the Pianec grabens complex south of Kjustendil. Structural stages. Bulletin of the Geological Institute, Series Geotectonics, Stratigraphy and Lithology 17, 143–158 (in Russian).
Moskovski, S., 1969. Tektonik eines Teiles des Pijanec-Grabenkomplexes südlich von Kjustendil Störungen. Annual of the Sofia University, vol. 1. Faculty of Geology and Geography, pp. 141–156 (in Bulgarian, with German abstract).
Moskovski, S., Harkovska, A., 1973. Main stages in the Late Alpine development of some fault zones in a part of South-Western Bulgaria. Annual of the Sofia University, vol. 1. Faculty of Geology and Geography, pp. 73–84 (in Bulgarian, with English abstract).
Moskovski, S., Shopov, V., 1965. Stratigraphy of the Paleogene and the resedimentation phenomena (olistostromes) related to it in Pyanets area, Kjustendil district (SW Bulgaria). Bulletin of the Institute of Geology, Stratigraphy and Lithology 16, 189–209 (in Bulgarian, with English abstract).
Mountrakis, D., Tranos, M., Papazachos, C., Thomaidou, E., Karagianni, E., Vamvakaris, D., 2006. New neotectonic and seismological data about the main active faults and stress regime of Northern Greece. Journal of Geological Society, London, 649–670 (Special Publications 260).
Mposkos, E., Krohe, A., 2000. Petrological and structural evolution of continental high pressure (HP) metamorphic rocks in the Alpine Rhodope Domain (N. Greece). In: Panayides, I., Xenopontos, C., Malpas, J. (Eds.), Proceedings of the 3rd International Conference on the Geology of the Eastern Mediterranean (Nicosia, Cyprus). Geological Survey Nicosia, Cyprus, pp. 221–232.
Nagel, T.J., Schmidt, S., Janák, M., Froitzheim, N., Jahn-Awe, S., Georgiev, N., 2011. The exposed base of a collapsing wedge: The Nestos Shear Zone (Rhodope Metamorphic Province, Greece). Tectonics 30, http://dx.doi.org/10.1029/2010TC002815.
Nedjalkov, P., Kojumdgieva, E., Bozhkov, I., 1988. Sedimentation cycle in the Neogene grabens along Strouma valley. Geologica Balkanica 18 (2), 61–66.
Nemcok, M., Lisle, R.J., 1995. A stress inversion procedure for polyphase fault/slip data sets. J. Struct. Geol. 17, 1445–1453.
Pamić, J., Balenb, D., Herak, M., 2002. Origin and geodynamic evolution of Late Paleogene magmatic associations along the Periadriatic–Sava–Vardar magmatic belt. Geodinamica Acta 15, 2090–2231.
Papadimitriou, E., Karakostas, V., Tranos, M., Ranguelov, B., Gospodinov, D., 2006. Static stress changes associated with normal faulting earthquakes in South Balkan area. International Journal of Earth Sciences (Geol Rundsch) 96, 911–924, http://dx.doi.org/10.1007/s00531-006-0139-x.
Pavlides, S.B., Kilias, A.A., 1987. Neotectonic and active faults along the Serbo-Macedonian zone (Chalkidiki, N. Greece). Annales Tectonicae 1, 97–104.
Pavlides, S.B., Mountrakis, D.M., 1987. Extensional tectonics of northwestern Macedonia, Greece, since the late Miocene. Journal of Structural Geology 9 (4), 385–392.
Petit, J.P., 1987. Criteria for the sense of movement on fault surfaces in brittle rocks. Journal of Structural Geology 9, 597–608.
Peychev, K., Kiselinov, H., Georgiev, S., Gorinova, T., Dimov, D., Georgiev, N., 2012. The Vlahina-Maleshevo Detachment Fault in Southwest Bulgaria – combined structural and zircon LA-ICPMS U-Pb study. In: National Conference with international participation GEOSCIENCES 2012, Bulgarian Geological Society, pp. 113–114.
Roussos, N., 1994. Stratigraphy and paleographic evolution of the Paleogene molassic basins of the North Aegean Sea. Bulletin of Geological Society of Greece 30 (2), 275–294 (in Greek with English abstract).
Royden, L.H., 1993. Evolution of retreating subduction boundaries formed during continental collision. Tectonics 12, 629–638, http://dx.doi.org/10.1029/92TC02641.
Saner, S., 1985. Sedimentary sequences and tectonic setting of Saros Gulf area: Northeast Aegean Sea, Turkey. Bulletin of the Geological Society of Turkey 28, 1–10 (in Turkish).
Schellart, W.P., Moresi, L., 2013. A new driving mechanism for backarc extension and backarc shortening through slab sinking induced toroidal and poloidal mantle flow: Results from dynamic subduction models with an overriding plate. Journal of Geophysical Research 118, 3221–3248, http://dx.doi.org/10.1002/jgrb.50173.
Simón Gómez, J.L., 1986. Analysis of a gradual change in stress regime (example from eastern Iberian Chain, Spain). Tectonophysics 124, 37–53.
Sinclair, H.D., Juranov, S.G., Georgiev, G., Byrne, P., Mountney, N.P., 1997. The Balkan thrust wedge and foreland basin of Eastern Bulgaria: Structural and stratigraphic development. In: Robertson, A.G. (Ed.), Regional and Petroleum Geology of the Black Sea and Surrounding Region. AAPG Memoir, pp. 91–114, 68.
Sokoutis, D., Brun, J.P., Van Den Driessche, J., Pavlides, S., 1993. A major Oligo-Miocene detachment in southern Rhodope controlling north Aegean extension. Journal of Geological Society of London 150, 243–246.
Tranos, M.D., (Ph.D. thesis) 1998. Contribution to the study of the neotectonics deformation in the region of Central Macedonia and North Aegean. University of Thessaloniki (in Greek with extended English abstract).
Tranos, M.D., 2004. Late Cenozoic faulting deformation of SW Bulgaria. In: Chatzipetros, A.A., Pavlides, S.B. (Eds.), 5th International

Symposium on Eastern Mediterranean Geology. Thessaloniki, Greece, 1, pp. 400–403.
Tranos, M.D., 2009. Faulting of Lemnos Island; a mirror of faulting of the North Aegean Trough (Northern Greece). Tectonophysics 467, 72–88, http://dx.doi.org/10.1016/j.tecto.2008.12.018.
Tranos, M.D., 2011. Strymon and Strymonikos Gulf basins (Northern Greece): implications on their formation and evolution from faulting. Journal of Geodynamics 51, 285–305, http://dx.doi.org/10.1016/j.jog.2010.10.002.
Tranos, M.D., 2012. Slip preference on pre-existing faults: a guide tool for the separation of heterogeneous fault slip data in extensional stress regimes. Tectonophysics 544–545, 60–74, http://dx.doi.org/10.1016/j.tecto.2012.03.032.
Tranos, M.D., 2013. The TR method: the use of slip preference to separate heterogeneous fault-slip data in compressional stress regimes. The surface rupture of the 1999 Chi-Chi Taiwan earthquake as a case study. Tectonophysics 608, 622–641, http://dx.doi.org/10.1016/j.tecto.2013.08.017.
Tranos, M.D., Eleftheriadis, G.E., Kilias, A.A., 2009. Philippi granitoid as a proxy for the Oligocene and Miocene crustal deformation in the Rhodope Massif (Eastern Macedonia, Greece). Geotectonic Research 96 (1), 69–85, http://dx.doi.org/10.1127/1864-5658/09/96-0069.
Tranos, M.D., Kachev, V.N., Mountrakis, D.M., 2008. Transtensional origin of the NE-SW Simitli basin along the Strouma (Strymon) Lineament, SW Bulgaria. Journal of the Geological Society, London 165, 1–12.
Tranos, M.D., Karakostas, V.G., Papadimitriou, E.E., Vladislav, N., Kachev, V.N., Ranguelov, B.K., Gospodinov, D.K., 2006. Major active faults of SW Bulgaria: implications of their geometry, kinematics and the regional active stress regime. Journal of Geological Society, London 260, 671–687 (Special Publications).
Tranos, M.D., Kilias, A.A., Mountrakis, D.M., 1999. Geometry and kinematics of the Tertiary post-metamorphic Circum Rhodope Belt Thrust System (CRBTS), Northern Greece. Bulletin of Geological Society of Greece 33, 5–16.
Turgut, S., Eseller, G., 2000. Sequence stratigraphy, tectonics and depositional history in eastern Thrace Basin, NW, Turkey. Marine and Petroleum Geology 17, 61–100, http://dx.doi.org/10.1016/S0264-8172(99)00015-X.
Van Hinsbergen, D.J.J., Dupont-Nivet, G., Nakov, R., Oud, K., Panaiotu, C., 2008. No significant post-Eocene rotation of the Moesian Platform and Rhodope (Bulgaria): implications for the kinematic evolution of the Carpathian and Aegean arcs. Earth and Planetary Science Letters 273, 345–358.
Vrablianski, B., 1974. Neotectonic studies in the Simitli graben and its framework. Bulletin of the Geological Institute, Geotectonics 23, 195–220 (in Bulgarian, with French summary).
Wawrzenitz, N., Krohe, A., 1998. Exhumation and doming of the Thasos metamorphic core complex (S Rhodope, Greece): structural and geochronological constraints. Tectonophysics 285 (3–4), 301–332, http://dx.doi.org/10.1016/S0040-1951(97)00276-X.
Westaway, R., 2006. Late Cenozoic extension in SW Bulgaria: a synthesis. Journal of Geological Society, London 260, 557–590 (Special Publications).
Yamaji, A., 2000. The multiple inverse method: a new technique to separate stresses from heterogeneous fault-slip data. Journal of Structural Geology 22, 441–452.
Zagorchev, I.S., 1989. Geological map of the People's Republic of Bulgaria, scale 1:100 000 series, Delchevo Sheet. Committee of Geology, Sofia.
Zagorchev, I.S., 1991. Geological map of the People's Republic of Bulgaria, scale 1:100 000 series, Kriva Palanka and Kyustendil Sheet. Committee of Geology, Sofia.
Zagorchev, I.S., 1992. Neotectonic development of the Strouma (Kraištid) Lineament, southwest Bulgaria and northern Greece. Geological Magazine 129 (2), 197–222.
Zagorchev, I.S., 2001. Introduction to the geology of SW Bulgaria. Geologica Balkanica 31 (1–2), 3–52.